https://doi.org/10.5194/egusphere-2026-791
Preprint. Discussion started: 10 April 2026

Representation of the nitrogen cycle and its coupling with the carbon cycle in ISBA (SURFEX v9) the land surface model: evaluation using two Free-Air CO_2 Enrichment experiment sites.

Jeanne Decayeux[1], Bertrand Decharme[1], Romain Darnajoux[2], and Christine Delire[1]

[1]Météo-France, CNRS, Univ. Toulouse, CNRM, Toulouse, France.
[2]Centre de Recherche sur la Biodiversité et l'Environnement (CRBE), Université de Toulouse, CNRS, IRD, Toulouse INP, Toulouse, France

Correspondence: Jeanne Decayeux (jeanne.decayeux@meteo.fr)

Abstract. Nitrogen (N) is a critical nutrient, that controls photosynthesis and decomposition processes. It is important to include the N cycle in the land component of climate models to improve the exchange fluxes of CO_2 between land and atmosphere. We present here the implementation of the N cycle in the CNRM land surface model, namely ISBA. We evaluate the model on two Free-Air Enrichment (FACE), experiments sites: Duke and Oak Ridge. In particular, the response to elevated CO_2 is studied. We compare the reference version without the N cycle (C) and the new version in which it is included (CN). A comparison to a multi model analysis shows encouraging results, since the computed NPP and N assimilation flux fall in the inter model range. The CN version performs better than the C version for NPP. Next, we focus on the carbon cycle by confronting simulation results to observations. The CN version improves the carbon stocks, largely overestimated by the C version. In particular, at elevated CO_2, in the CN version, photosynthesis is downregulated by the N limitation. This yields a reduction of C accumulation in soil and biomass in comparison to the C version. In the literature, diverging strategies are observed to overcome N limitation. The model reproduces well the main features but fails to represent some sites characteristics. Finally, a detailed analysis of the simulated N dynamics is presented.

1 Introduction

Climate change is driven by anthropogenic emissions of greenhouse gases, such as CO_2, to the atmosphere, which disturbs the natural carbon (C) cycle. Rising atmospheric CO_2 concentration exerts a fertilization effect by stimulating photosynthesis, causing land ecosystems to act as a C sink. This leads to an increase in C storage in terrestrial ecosystems (Pan et al., 2011; Tagesson et al., 2020; Sitch et al., 2024). This C sink plays a crucial role in mitigating the impact of human emissions, absorbing roughly one-third of the total CO_2 emissions (Friedlingstein et al., 2024). However, its long term fate is uncertain because the CO_2 fertilization effect depends on the availability of water and nutrients, and is constrained by disturbances including fires and

https://doi.org/10.5194/egusphere-2026-791
Preprint. Discussion started: 10 April 2026

disease (Elser et al., 2007; Fleischer and Terrer, 2022). In particular, nitrogen availability has been pointed out as a first order limiting factor on the carbon cycle (Vitousek and Howarth, 1991; Flechard et al., 2020). Nitrogen is a key nutrient for plant growth and for organic matter decomposition processes (Schlesinger, 1997; Parton et al., 1988), and long term enhanced CO_2 concentration is expected to lead to a progressive nitrogen limitation (Johnson, 2006). Reduced nitrogen availability occurs as nitrogen becomes increasingly immobilized in plant and soil organic matter, leading to lower mineral nitrogen availability for further plant uptake (Luo et al., 2004). Plants and ecosystems may partially compensate for this limitation through changes such as increased nitrogen-use efficiency (NUE), higher C:N ratios, and greater fine-root production to access additional nutrients.

Earth system models (ESMs) are used to predict future climate in response to human activity and continued CO_2 emissions (Voldoire et al., 2019). They include land surface components that may be run in an offline mode using atmospheric forcings to analyze the evolution of the land surface C sink (Sitch et al., 2024). Without representation of N constraints on the C cycle, the C uptake may be unrealistically overestimated (Wieder et al., 2015b). Therefore, modelers recently included an explicit nitrogen cycle coupled to the carbon cycle, allowing C-N interactions and feedbacks to be investigated under climate change and rising CO_2 (Goll et al., 2012; Thornton et al., 2007; De Sisto et al., 2023). On average, models including a nitrogen cycle predict a lower land carbon sink than models without one (Arora et al., 2020). Nevertheless, the range of modeled carbon stocks is wider (Stocker et al., 2025), reflecting the complexity of the processes involved (Meyerholt et al., 2020; Wieder et al., 2015a). Moreover, there is a lack of observations to constrain these models (Kou-Giesbrecht et al., 2023).

ISBA, for Interaction-Soil-Biosphere-Atmosphere, is the land surface component of the CNRM earth system model (ESM) Séférian et al. (2019). The model is used for future projections inluding the Climate Model Intercomparison Project (CMIP) (Voldoire et al., 2019). It can be used interactively with the other components of the ESM, or in an offline mode using prescribed atmospheric forcings. ISBA represents the surface energy, water and carbon budgets. A dynamic C cycle is already implemented (Delire et al., 2020; Decharme et al., 2019; Morel et al., 2019; Gibelin et al., 2008) with an implicit nitrogen limitation (Yin, 2002). Despite this parametrization, the model remains too responsive to the elevated CO_2. An additional tuning was therefore implemented to obtain more realistic future C uptake projections (Delire et al., 2020). However, both of these N limitations are not process-based and feedbacks to rising CO_2 emissions are not well represented. To address this issue more mechanistically, a comprehensive nitrogen cycle needed to be implemented.

In this paper, we present the implementation of an explicit N cycle in ISBA. The approach follows developments made in other land surface models such as ORCHIDEE, JSBACH, QUINCY, JULES (Vuichard et al., 2019; Reick et al., 2021; Thum et al., 2019; Wiltshire et al., 2021). The representation of the nitrogen cycle is built consistently with the carbon cycle. C and N dynamics are coupled through stoichiometric ratios between C and N pools and by imposing nitrogen limitation on carbon assimilation and decomposition processes.

To evaluate model performance, we use data from the Free-Air CO_2 Enrichment (FACE) experiments conducted over 10 years in North America (Hendrey et al., 1999; McCarthy et al., 2010; Norby et al., 2002). These experiments, which impose an elevated atmospheric CO_2 in field conditions, provide a good framework to test the ability of the updated model to represent nutrient constraints on CO_2 fertilization (Finzi et al., 2002, 2007; Zaehle et al., 2014; Norby et al., 2010; Drake et al., 2011). We compare our model simulations to site observations and to the results of a model intercomparison exercise conducted at

https://doi.org/10.5194/egusphere-2026-791
Preprint. Discussion started: 10 April 2026

these two sites. We then assess the ISBA carbon cycle at the two FACE sites and evaluate the impact of adding the nitrogen cycle. Finally, we analyze the internal dynamics of the nitrogen cycle in the model and discuss further improvements.

2 Implementation of the nitrogen cycle in the ISBA land surface scheme

2.1 The carbon dynamics in ISBA

ISBA is embedded in the SURFEX modeling platform. The current version is SURFEX V9.1, described in Delire et al. (2020); Decharme et al. (2019); Morel et al. (2019). ISBA uses a 14-layer scheme to solve soil physics (hydrology, thermodynamics, gas diffusion). The model includes the representation of 16 plant functional types (PFTs), rock, ice and bare soil. The ISBA scheme used here is ISBA-CC described in Gibelin et al. (2008). This version computes carbon cycle dynamics using 6 pools to represent plants and 7 pools for the soil organic matter. Photosynthesis is represented using a semi-empirical approach based on Jacobs (1994), implemented by Calvet et al. (1998). The scheme was modified by Joetzjer et al. (2015) for tropical vegetation. As previously stated, an implicit nitrogen limitation was implemented to regulate photosynthesis with increasing CO_2. It consists of two parameterizations: the first one acts globally to correct the model tendency to overestimate CO_2 fertilization. The second acts directly on photosynthesis by reducing the specific leaf area (SLA) with increasing CO_2, thereby constraining leaf growth and carbon assimilation (Delire et al., 2020).

The assimilated carbon is first allocated to the leaves. It is then reallocated to the other biomass pools using different empirical allometric relations (Gibelin et al., 2008). Each biomass carbon pool is associated with a respiration and a turnover rate. Soil litter and soil organic-carbon pools are represented within each soil layer, and their dynamics follow the CENTURY model of Parton et al. (1988). Latest developments include a gas module that explicitly simulates the dynamics of O_2, CO_2, and CH_4 (Morel et al., 2019) with methane related processes and vertical carbon transfers. The equations driving the carbon cycle are detailed in the Appendix A.

2.2 Implementation of a N cycle within the carbon dynamics in ISBA

We chose to build the nitrogen cycle consistently with the carbon cycle. Each vegetation and soil carbon pool has an associated nitrogen pool, and nitrogen decomposition fluxes follow those of carbon (Fig. 1). To reduce computational cost, these N pools and fluxes are not explicitly represented, consistent with approaches used in other land models (Jain et al., 2009; Zaehle and Friend, 2010; Vuichard et al., 2019; Wiltshire et al., 2021). Instead carbon and nitrogen pools are linked by stoichiometric nitrogen-carbon ratios (N/C) that are prescribed for all pools except for leaves in order to adjust vegetation response to N availability (Zaehle and Friend, 2010; Vuichard et al., 2019; Wiltshire et al., 2021). The model also explicitly describes the dynamics of a labile nitrogen pool in vegetation and a mineral nitrogen pool in soils. Soil and vegetation exchange N by an uptake flux that is a function of the mineral N availability, root distribution and plant N demand (Yang et al., 2009; Jain et al., 2009; Vuichard et al., 2019; Zaehle and Friend, 2010). Consequently, a limitation in the N mineral pool directly reduces plant

https://doi.org/10.5194/egusphere-2026-791
Preprint. Discussion started: 10 April 2026

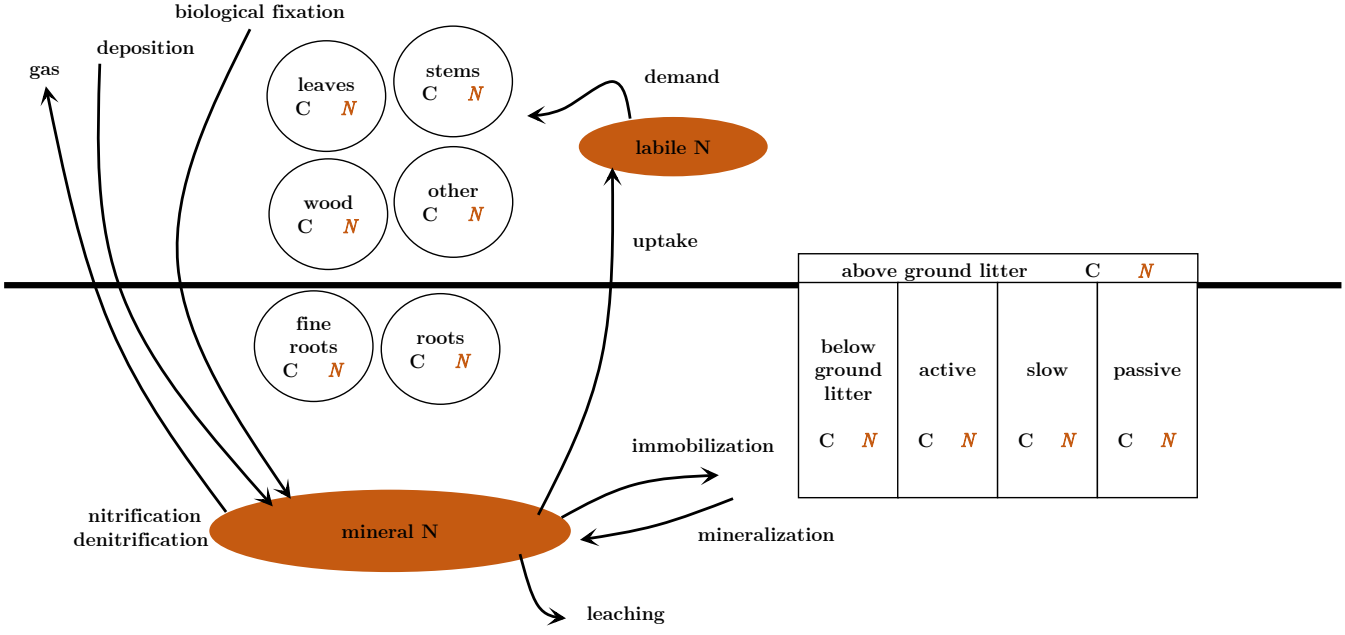

Figure 1. Schematic representation of the C and N cycle. Pools representing biomass and soil, in black existing carbon pools, in brown the newly added nitrogen pools. In italic pools which dynamics is represented implicitly. Only process linked to nitrogen cycle are represented by the arrows.

NPP, and constrains the decomposition of organic matter. Gazeous exchanges with the atmosphere and leaching of mineral N are also represented.

2.3 Labile nitrogen

The labile pool of nitrogen, N_{labile}, is a storage pool that represents the nitrogen that is easily transported within the plant (Tegeder and Masclaux-Daubresse, 2018). N is taken up from the soil by the roots and is then redistributed to the various plant parts. Its dynamics is explicitly represented by:

$$\frac{\mathrm{d}}{\mathrm{d}t} N_{\text{labile}}(t) = N_{\text{upday}}(t) - N_{\text{demand}}(t) \tag{1}$$

where N_{upday} represents the nitrogen taken up by plants from the soil mineral reservoir (see Sect. 2.6) and N_{demand} is the nitrogen needed to build plant tissues. Because the C allocation scheme in ISBA is built as a cascade through the biomass pools with multiple outcomes (see Appendix A), the computation of the N needed to fulfill tissue growth is diagnosed by comparing the total biomass before and after C allocation and applying the corresponding N/C ratio. However, this diagnosed flux needs

https://doi.org/10.5194/egusphere-2026-791
Preprint. Discussion started: 10 April 2026

to be corrected by turnover because the change in total biomass results from both tissue growth and turnover while only growth implies a N demand.

$$N^*_{\text{demand}} = \frac{1}{\Delta t}\sum_{x=1}^{6}[B^*_x(t+\Delta t) - B_x(t)] \times NC_{B_x} + N^*_{\text{turn}}(t) \tag{2}$$

where NC_{B_x} is the N/C ratio of the biomass pool x and N^*_{turn} is the N lost by turnover. To render the known N translocation of N from leaf to plant during senescence (Norby and Iversen, 2006; Finzi et al., 2002), the N turnover flux is reduced by a fraction that is directed from the leaf pool to the storage pool before leaf fall. This results in marked difference between C turnover and N turnover. This has the effect of decorrelating C and N turnover fluxes. N^*_{turn} is expressed as:

$$N^*_{\text{turn}}(t) = \sum_{x=1}^{6}(1 - f_{\text{trans},x})M_x(t)NC_{B_x} \tag{3}$$

where $f_{\text{trans},x}$ is the fraction of nitrogen from pool x that is translocated (see Table 1) and M_x the turnover rate of the C pool x. * denotes potential fluxes before N limitation that is described in Sect. 2.4. In these last 2 equations, NC_{B_x} is time dependent for leaves and prescribed for all other pools (see Sect.2.5). N demand can be positive: nitrogen is needed to meet carbon demand. However, the biomass cascade in the model is build so that carbon is transferred from metabolic pools (high N/C) to more ligneous pools (low N/C). As a consequence, the N demand can also be negative. In this case, the surplus of nitrogen is transferred to the labile pool. Similarly to the C allocation scheme, the dynamics of N_{labile} is computed once a day.

2.4 Nitrogen limitation in biomass

In response to N limitation, the photosynthesis is reduced which slows down tissue growth. In addition, the plant limit N losses by readsorbing more N during senescence. In the model, both strategies are implemented sequentially. The first step is to limit C assimilation. This is implemented by computing the C allocation scheme twice. The first time, the C allocation is computed considering infinite N supply. This gives the potential N^*_{demand} from eq. (2) and (3) that is compared to the available labile N to compute the limitation parameter, $\eta_{\text{lim,assim}}$, following Zaehle and Friend (2010):

$$\eta_{\text{lim,assim}} = \min\left(1, \frac{f_{\text{labile,max}}N_{\text{labile}}}{N^*_{\text{demand}}\Delta t}\right) \tag{4}$$

where $f_{\text{labile,max}} = 0.9$ is a limit to empty at most 90% of the labile pool. This limitation is immediately applied to the daily net carbon assimilation by leaves during the second round of computation of C allocation. $A_1(t) = \eta_{\text{lim,assim}}A^*_1(t)$. This updates all the biomass pools and the actual N demand.

$$N_{\text{demand}} = \frac{1}{\Delta t}\sum_{x=1}^{6}[B_x(t+\Delta t) - B_x(t)] \times NC_{B_x} + N^*_{\text{turn}}(t) \tag{5}$$

The limitation may persist. The second step is then to increase retranslocation from leaves to the labile pool, as it has been done in the FUN model developed by Fisher et al. (2010). A correction is applied to the nitrogen turnover flux if there is no sufficient

https://doi.org/10.5194/egusphere-2026-791
Preprint. Discussion started: 10 April 2026

N labile to support it. The corrective factor, f_{corr}, is computed as the ratio of the maximum quantity that can be removed from the labile pool ($f_{\mathrm{labile,max}} N_{\mathrm{labile}} - N_{\mathrm{demand}}$) and the potential turnover flux N^*_{turn}.

$$f_{\mathrm{corr}} = \min\left(1, \frac{f_{\mathrm{labile,max}} N_{\mathrm{labile}} - N_{\mathrm{demand}}}{N^*_{\mathrm{turn}}}\right) \tag{6}$$

The actual turnover is then $N_{\mathrm{turn}} = f_{\mathrm{corr}} N^*_{\mathrm{turn}}$.

2.5 Nitrogen carbon ratio

The nitrogen-carbon ratio evolves during the plant development and also in response to environmental constraints (Vitousek et al., 1988). It has been observed in general that (i) structural elements such as branches, bark or heartwood contain less nitrogen than leaves. (ii) Litter is N poor compared to vegetation biomass and soil organic carbon. As a first approximation, we assumed in the model the ratio to be constant for all pools except for leaves. We prescribe a PFT-dependent value adapted from literature (Vitousek et al., 1988; White et al., 2000). The ratio associated with each carbon pool is denoted by NC_{B_x}, for biomass pool B_x and NC_{C_i} for soil carbon pool C_i. Table B1 summarizes values used in the model. The leaf ratio, NC_{B_1}, varies in order to adjust the system to the nitrogen availability. Initial value is taken according literature. Then, it increases when the nitrogen supply matches the potential total demand $N^*_{\mathrm{demand}} > N_{\mathrm{labile}}$, otherwise it decreases. Minimum and maximum values are set to avoid unrealistic ratios (see Table B1). Variations of NC_{B_1} are described by equation (7), adapted from Vuichard et al. (2019).

$$NC_{B_1}(t+\Delta t) = \begin{cases} N_{\mathrm{labile}} < N^*_{\mathrm{demand}} : NC_{B_1}(t) \times \max\left(\frac{N_{\mathrm{labile}}}{N^*_{\mathrm{demand}}}, 1 - 0.25 \times \gamma_{\mathrm{NC}}\right) \\ N_{\mathrm{labile}} > N^*_{\mathrm{demand}} : NC_{B_1}(t) \times \min\left(\frac{N_{\mathrm{labile}}}{N^*_{\mathrm{demand}}}, 1.25 - 0.25 \times \gamma_{\mathrm{NC}}\right) \end{cases} \tag{7}$$

where γ_{NC} dampens the variation according to :

$$\gamma_{\mathrm{NC}} = \exp\left(-\left[\lambda \times \frac{NC_{B_1,\max} - NC_{B_1}(t)}{NC_{B_1,\max} - NC_{B_1,\min}}\right]^k\right) \tag{8}$$

The parameters $\lambda = 1.6$ and $k = 3.0$ are chosen arbitrarily to adjust the model.

2.6 Soil mineral nitrogen

Mineral (inorganic) N may be found as two soluble species in the soil: NH_4^+ and NO_3^- (Schlesinger, 1997). Nitrogen enters the soil system by biological N fixation (BNF), N_{bnf}, and by deposition, N_{depo}. Both are complex processes (Cleveland et al., 1999; Bellenger et al., 2020; Galloway et al., 2004; Lamarque et al., 2011) that are simplified and supposed to directly supply the mineral pool (see Sect. 2.6.1). Mineral nitrogen undergoes chemical reactions (nitrification and denitrification) during which N is lost to the atmosphere as gas, N_{gas}. N is also loss due to leaching towards river and oceans, N_{leaching} and by plants to fulfill growth, N_{up}. Decomposition processes are releasing nitrogen, but micro-organisms requires nitrogen to carry out their tasks. This is denoted by net mineralization , N_{netmin}. We represent the two ion species as one mineral pool N_{min} with

https://doi.org/10.5194/egusphere-2026-791
Preprint. Discussion started: 10 April 2026

associated fractions of NH_4^+ (f_{NH4}) and NO_3^- ($f_{NO_3} = 1 - f_{NH4}$), similarly to Reick et al. (2021). The soil N mineral pool is vertically discretized and its dynamics is computed on the same vertical grid as the soil water, temperature and carbon. Mineral N dynamics is described for each soil layer l by :

$$\frac{\mathrm{d}}{\mathrm{d}t} N_{\mathrm{min},l}(t) = N_{\mathrm{BNF}} f_{\mathrm{water},l} + N_{\mathrm{depo}} f_{\mathrm{water},l} - N_{\mathrm{gas},l} - N_{\mathrm{leaching},l} - N_{\mathrm{up},l} + N_{\mathrm{netmin},l} \tag{9}$$

Variables added to represent the soil N dynamics are summarized in Table E1, and the fluxes are detailed in the following sections.

2.6.1 External input

Biological fixation

For simplification, the various sources of biological fixation are not detailed. The idea is to model the entry of nitrogen without describing the complexity of the process. Based on Cleveland et al. (1999) approach, which states that biological fixation is proportional to NPP, the land surface model JULES used a linear correlation between BNF and NPP (Wiltshire et al., 2021). The same formulation is used here:

$$N_{\mathrm{BNF}} = k_{\mathrm{BNF}} \mathrm{NPP}, \tag{10}$$

where k_{BNF} is the rate of fixation in $\mathrm{g_N\ g_C^{-1}}$ and is set to match the global value of BNF observed per year (100 $\mathrm{Tg_N\ y^{-1}}$, Galloway et al. (2004)).

Deposition

Deposition is computed using a fixed rate k_{depo} in $\mathrm{g_N\ m^2\ s^{-1}}$ to match the annual deposition flux observed. In this study, we take observed values from Sparks et al. (2008); Norby et al. (2010) (see Table 1). Hence,

$$N_{\mathrm{depo}} = k_{\mathrm{depo}}. \tag{11}$$

The deposition is added to the mineral pool and is supposed to be immediately accessible for the biomass.

Approximation of diffusivity

The NH_4^+ and NO_3^- ions that form the N mineral pool are soluble and diffuse in water (Schlesinger, 1997). To mimic the result of this diffusion that is not currently represented in ISBA, the BNF and deposition input fluxes are spread per layer according to the water vertical profile:

$$f_{\mathrm{water},l} = \frac{w_{\mathrm{g},l} \Delta z_l}{\sum_{l=1,l_{\mathrm{bottom}}} w_{\mathrm{g},l} \Delta z_l} \tag{12}$$

where $w_{\mathrm{g},l}$ is the soil liquid water content of layer l in $\mathrm{m^3\ m^{-3}}$, Δz_l is the layer thickness in m and l_{bottom} the last soil layer.

https://doi.org/10.5194/egusphere-2026-791
Preprint. Discussion started: 10 April 2026

2.6.2 Gas losses

Numerous chemical reactions occur in the soil, transforming nitrogen species from one form into another. The two main reactions are nitrification and denitrification and are both represented in the model. During nitrification, NH_4^+ is oxidized in NO_3^- and denitrification transforms NO_3^- into N_2 that is released to the atmosphere. During these reactions, other species are emitted as by-products such as N_2O and NO, both being greenhouse gases of interest. Nitrification needs oxygen to occur, whereas denitrification occurs only in anaerobic conditions. Both reactions can take place at the same time and place because the soil contains micropores that have different water saturation status.

As a first step, the aim is to quantify the inorganic losses as gases. Later, diffusion of gases will be described and each gas species will be tracked down following the work of Morel et al. (2019). The modeling of gas losses is based on the QUINCY model (Thum et al., 2019). We divide the soil by defining an anaerobic fraction that is a key parameter to represent denitrification and nitrification as discussed in Schlüter et al. (2025). In this model, we will use a simplified scheme that do not account for the soil heterogeneity. Since we have access to the simulated concentration profile in the soil of O_2, we follow a similar approach of Li et al. (2000). We modify the function used in this paper according to Thum et al. (2019) to account for a more abrupt transition between anaerobic and aerobic.

$$f_{\text{anaero},l} = \exp\left(-\lambda_{\text{nit}} \times \frac{p_{O_2,\text{soil},l}}{p_{\text{soil},l}}\right) \tag{13}$$

where $p_{O_2,\text{soil},l}$ is the O_2 partial pressure in soil at layer l and $p_{\text{soil},l}$, the total soil pressure at layer l. O_2 pressure is derived from the O_2 concentration computed by using the gas module implemented in the latest ISBA version as described by Morel et al. (2019). The equation is designed to suppress nitrification below a partial pressure of oxygen of 0.5 % relatively to the soil pressure Li et al. (2000), Table 1 references parameters units and values.

Nitrification

Nitrification is represented as a fixed maximum rate, $v_{\text{max,nit}}$, of NH_4^+ being transformed into NO_3^-. The reaction takes place in the aerobic part of soil, $(1 - f_{\text{anaero},l})$. The flux is corrected by temperature and soil moisture functions described in Appendix C1.

$$N_{\text{nit},l} = v_{\text{max,nit}} f_{\text{NH4}} N_{\text{min},l} \left(1 - f_{\text{anaero},l}\right) f(\theta_l) f(T_l). \tag{14}$$

Parameters used are referenced in Table 1.

Denitrification

According to Li et al. (2000); Thum et al. (2019), denitrification can be modeled as Michaelis-Menten functions of the NO_3^- and soluble C pools (corresponding in ISBA to the active carbon pool C_1). There is a fixed maximum rate of mineral N

https://doi.org/10.5194/egusphere-2026-791
Preprint. Discussion started: 10 April 2026

denitrified $v_{\max,\text{denit}}$, corrected by a function of temperature $f(T_l)$ described in Appendix C2.

$$N_{\text{denit},l} = v_{\max,\text{denit}} f(T_l) \frac{C_{1,l}}{K_{\text{denit,C}}\Delta z_l + C_{1,l}} \frac{f_{\text{NO3}} N_{\text{min},l}}{K_{\text{denit,N}}\Delta z_l + f_{\text{NO3}} N_{\text{min},l}} f_{\text{anaero},l}\ f_{\text{NO3}} N_{\text{min},l} \tag{15}$$

Parameters are described in Table 1.

Gas output

During both the nitrification and denitrification processes, NO_y and N_2O gases are lost as by-products. Denitrification ultimately releases N_2. Prescribed fractions derived from observations (Khalil et al., 2004; Parton et al., 1996), are used to compute the flux of each gas:

$$\begin{aligned} N_{\text{NO}_y,l} &= f_{\text{nit,NO}_y} N_{\text{nit},l} + f_{\text{denit,NO}_y} N_{\text{denit},l} \\ N_{\text{N}_2\text{O},l} &= f_{\text{nit,N}_2\text{O}} N_{\text{nit},l} + f_{\text{denit,N}_2\text{O}} N_{\text{denit},l} \\ N_{\text{N}_2,l} &= (1 - f_{\text{denit,NO}} - f_{\text{denit,N}_2\text{O}})\, N_{\text{denit},l} \end{aligned} \tag{16}$$

As a result, the total gas loss from the mineral pool to the atmosphere comes from the by-products of the nitrification reaction and the entire denitrification flux:

$$N_{\text{gas},l} = f_{\text{nit,NO}_y} N_{\text{nit},l} + f_{\text{nit,N}_2\text{O}} N_{\text{nit},l} + N_{\text{denit},l} \tag{17}$$

2.6.3 Nitrogen leaching

We assume that nitrogen is leaching at the same rate k_{drain} as water drainage:

$$k_{\text{drain}} = \frac{F_{\text{drain}}}{w_{\text{g},l_{\text{bottom}}} \rho_{\text{w}} \Delta z_{l_{\text{bottom}}}} \tag{18}$$

where F_{drain} is the drainage flux at the bottom of the soil column in kg m^{-2} s^{-1}, $w_{\text{g},l_{\text{bottom}}}$ the water content of the bottom soil layer in m^3 m^{-3}, ρ_{w} the water density in kg m^{-3} and $\Delta z_{l_{\text{bottom}}}$ the bottom soil layer thickness. Total N loss is then $k_{\text{drain}} N_{\text{min}}$. To compensate the fact that the vertical transport of N_{min} is not represented, the N leaching flux is removed from each layer :

$$N_{\text{leaching},l} = k_{\text{drain}} N_{\text{min},l} \tag{19}$$

2.6.4 Nitrogen uptake

$$N_{\text{up},l} = v_{\max,\text{up}}\ N_{\text{min},l} \left(k_{\text{Nup}} + \frac{1}{N_{\text{min},l} + K_{\text{Nup}}} \right) f(T_l) f(NC_{\text{leaf}})\ f_{\text{root},l} B_4 \tag{20}$$

Plant nitrogen uptake is described by equation (20) following work of Zaehle and Friend (2010). The uptake flux is a growing function of the roots density ($f_{\text{root},l} B_4$ with $f_{\text{root},l}$ the root fraction in layer l) and has a Michaelis-Menten dependency on the size of the mineral pool. The flux is computed for each soil layer l. Its temperature dependency $f(T_l)$ is a Q_{10} function as for the decomposition processes. The flux is a function of the plant N status, described by equation (21): the more nitrogen content in the plant the less nitrogen uptake and vice-versa.

$$f(NC_{B_1}) = \max\left(0, \frac{NC_{B_1}(t) - NC_{B_1,\max}}{NC_{B_1,\min} - NC_{B_1,\max}}\right) \tag{21}$$

https://doi.org/10.5194/egusphere-2026-791
Preprint. Discussion started: 10 April 2026

Soil dynamics is computed at the model timestep, therefore the uptake flux from soil layer l $N_{\mathrm{up},l}$ is summed throughout the day to be used for the biomass dynamics. It is also summed through all layers. N_{upday} is the resulting flux defined by,

$$N_{\mathrm{upday}} = \sum_t \sum_l N_{\mathrm{up},l,t} \Delta t. \tag{22}$$

2.6.5 Net mineralization

During the decomposition process, nitrogen contained in the plant tissue is mineralized. Conversely, micro-organisms require nitrogen to carry out their decomposition tasks. In particular, the decomposition of litter, which is poor in nitrogen, immobilizes mineral nitrogen (Schlesinger, 1997). In the model, this is represented by a nitrogen flux associated with each carbon decomposition flux following Parton et al. (1988). The flux can be positive if nitrogen is mineralized, corresponding to a carbon transfer from a high nitrogen content pool to a pool with a lower nitrogen content. If the flux is negative, nitrogen is immobilized from the mineral pool to support the decomposition process. This happens when carbon is transferred from a low nitrogen content pool to a higher nitrogen content pool. Respiration due to decomposition is associated to mineralization of nitrogen. Nitrogen fluxes associated to carbon decomposition are the following:

- $F_{B_x,L_{\mathrm{surf}}}$ is the aboveground biomass pool turnover (B_x, $x \in \{1,2,3,5\}$) becoming the surface litter (C_1 and C_2). This flux is divided on the first four soil layers using a weight ratio $w_{N_{\mathrm{min}},l}$ computed by equation (24).
- $F_{B_x,L_{\mathrm{soil}}}$ is the belowground biomass pool (roots) turnover (B_x, $x \in \{4,6\}$) becoming the soil litter (C_3 and C_4). The turnover is distributed to the soil according the root profile.
- $F_{L_{\mathrm{surf}},\mathrm{SOC}}$ is the decomposition from surface litter (C_1 and C_2) to SOC pools (C_i, $i \in \{5,6,7\}$). This flux is divided on the first 4 soil layers using a weight ratio $w_{N_{\mathrm{min}},l}$ computed by equation (24).
- $F_{L_{\mathrm{soil}},\mathrm{SOC},l}$ is the decomposition in layer l from soil litter (C_3 and C_4) to SOC pools (C_i, $i \in \{5,6,7\}$)
- $F_{\mathrm{SOC},l}$ is the decomposition in layer l of SOC pools (C_i, $i \in \{5,6,7\}$).

Net mineralization is the resultant flux computed by:

$$N_{\mathrm{netmin},l} = F_{B_x,L_{\mathrm{surf}}} w_{N_{\mathrm{min}},l} + F_{B_x,L_{\mathrm{soil}}} f_{\mathrm{root},l} + F_{L_{\mathrm{surf}},\mathrm{SOC}} w_{N_{\mathrm{min}},l} + F_{L_{\mathrm{soil}},\mathrm{SOC},l} + F_{\mathrm{SOC},l} \tag{23}$$

where $w_{N_{\mathrm{min}},l}$ is the weight ratio to separate the aboveground biomass turnover and the surface litter decomposition to the first 4 soil layers:

$$w_{N_{\mathrm{min}},l} = \frac{N_{\mathrm{min},l}}{\sum_{k=1}^{4} N_{\mathrm{min},k}} \tag{24}$$

Further details on the computation of this fluxes can be found in Appendix D.

https://doi.org/10.5194/egusphere-2026-791
Preprint. Discussion started: 10 April 2026

2.6.6 Soil nitrogen limitation

Each flux that removes N from the N mineral pool can be limited if there is not enough mineral N to support it. Due to the code construction, net mineralization is computed first, and is thus prioritized in case of N deficit. This is not in contradiction with observations (Finzi et al., 2002). N limitation on the decomposition process depends on the decomposition process considered:

1. Decomposition of biomass:
   The code is constructed so that decomposition of biomass should lead to N mineralization. Indeed, N/C ratios of biomass pools are higher than the litter ones. However, when N_{labile} is very low, N turnover may be strongly reduced by translocation (see Sect. 2.4) leading to an effective N/C ratio for the turnover flux that can be lower than N/C ratio of litter. This can lead to a critical situation if there is not enough mineral N to support it. This situation is in practice very rare. We chose for numerical reasons to allow for a provisional N deficit that is retrieved from the N mineral pool as soon as possible during the next time steps to ensure a closed budget.

2. Other decomposition processes:
   The immobilization flux F is computed from the potential flux F^* by applying the limitation as $F = F^* \eta_{\text{lim,decomp},l}$, where

$$\eta_{\text{lim,decomp},l} = \min\left(1.0, \frac{N_{\text{min},l}}{F^*}\right). \tag{25}$$

   The limitation is also applied to the carbon decomposition flux $F_{\text{oxic},i,l}$ to maintain the N/C ratio of the pool. For decomposition of surface litter the limitation is modified to compare the flux to the N content of the first four layers.

$$\eta_{\text{lim,decomp}} = \min\left(1.0, \frac{\sum_{k=1}^{4} N_{\text{min},k}}{F^*}\right) \tag{26}$$

The limitation is then done on the other mineral N output fluxes by comparing the mineral N available and the sum of all fluxes that empty the mineral N pool:

$$\eta_{\text{lim,soil},l} = \min\left(1.0, \frac{N_{\text{min},l}}{\Delta t(N^*_{\text{gas},l} + N^*_{\text{up},l} + N^*_{\text{leaching},l})}\right). \tag{27}$$

Similarly, the final output fluxes are computed by applying the limitation to the potential output fluxes N^*.

3 Methods

3.1 Evaluation sites: Duke forest and Oak Ridge

The model is evaluated on two Free-Air CO_2 enrichment (FACE), experiment sites located in North America: Duke and Oak Ridge forests. Figure 2 exhibits the mean seasonal temperature and precipitation at Duke and Oak Ridge. Both sites present a

https://doi.org/10.5194/egusphere-2026-791
Preprint. Discussion started: 10 April 2026

Symbols	Value	Units	Reference
NC_{B_x}, NC_{C_i} $NC_{B_1,\max}$, $NC_{B_1,\min}$	see Table B1	unitless	
k	3.0	unitless	This study
λ	1.6	unitless	Vuichard et al. (2019)
$f_{\text{trans},1}$, $f_{\text{trans},x}$, $x \in [2,6]$	0.5, 0	unitless	Zaehle and Friend (2010)
$f_{\text{labile,max}}$	0.9	unitless	This study
k_{BNF}	0.0016	$g_N\ g_C^{-1}$	Wiltshire et al. (2021)
k_{depo}	4.4×10^{-8}	$g_N\ m^{-2}\ s^{-1}$	Sparks et al. (2008); Norby et al. (2010)
λ_{nit}	0.02	unitless	This study
$v_{\max,\text{nit}}$	4.63×10^{-6}	s^{-1}	Thum et al. (2019)
f_{NH_4}	0.4	unitless	Reick et al. (2021)
f_{NO_3}	0.6	unitless	Reick et al. (2021)
$v_{\max,\text{denit}}$	1.16×10^{-6}	s^{-1}	Thum et al. (2019)
$K_{\text{denit,C}}$	17	$g_C\ m^{-3}$	Xu-Ri and Prentice (2008)
$K_{\text{denit,N}}$	83	$g_N\ m^{-3}$	Xu-Ri and Prentice (2008)
f_{nit,NO_y}	0.02	-	Thum et al. (2019)
f_{nit,N_2O}	0.002	-	Thum et al. (2019)
f_{denit,NO_y}	0.002	-	Thum et al. (2019)
f_{denit,N_2O}	0.02	-	Thum et al. (2019)
$k_{N_{\text{up}}}$	0.05	$m^2\ g_N^{-1}$	Zaehle and Friend (2010)
$K_{N_{\text{up}}}$	0.83	$g_N\ m^{-2}$	Zaehle and Friend (2010)
$v_{\max,\text{up}}$	8.28×10^{-9}	$g_N\ g_C^{-1}\ d^{-1}$	adapted from Zaehle and Friend (2010); Kronzucker et al. (1996)

Table 1. Parameters used for the implementation of the N cycle

similar climate. The average annual temperature and precipitation are: 15.5 °C and 1140 mm at Duke (Lichter et al., 2005) and 13.9 °C and 1371 mm at Oak Ridge (Johnson et al., 2004).

The Duke experiment was conducted in a pine forest in North Carolina (35°58' N, 79°06' W). The stand is composed of 92% loblolly pine (*Pinus taeda*), with sub-dominant sweetgum and yellow poplar trees, and forty-eight other woody plant species (Hamiton et al., 2002). The forest was established in 1983 and the experiment began in 1996 (Lichter et al., 2005). Six circular plots, each 30 meters in diameter, were studied. Half were used as control plots and were exposed to ambient CO_2 concentration, (aCO_2: 350 ppm), while the other three received elevated CO_2 concentration (eCO_2: 571 ppm) (Hamiton et al., 2002).

Oak Ridge forest is composed of sweetgum (*Liquidambar styraciflua* L.) and is located in Tennessee (35°54' N, 84°20' W). Trees were planted in 1988, and the experiment began in 1997 (Norby and Iversen, 2006). The plots each have a diameter of 25 meters. There are two control (aCO_2: 390 ppm) and three elevated CO_2 plots (eCO_2: 542 ppm) (Jastrow et al., 2005).

https://doi.org/10.5194/egusphere-2026-791
Preprint. Discussion started: 10 April 2026

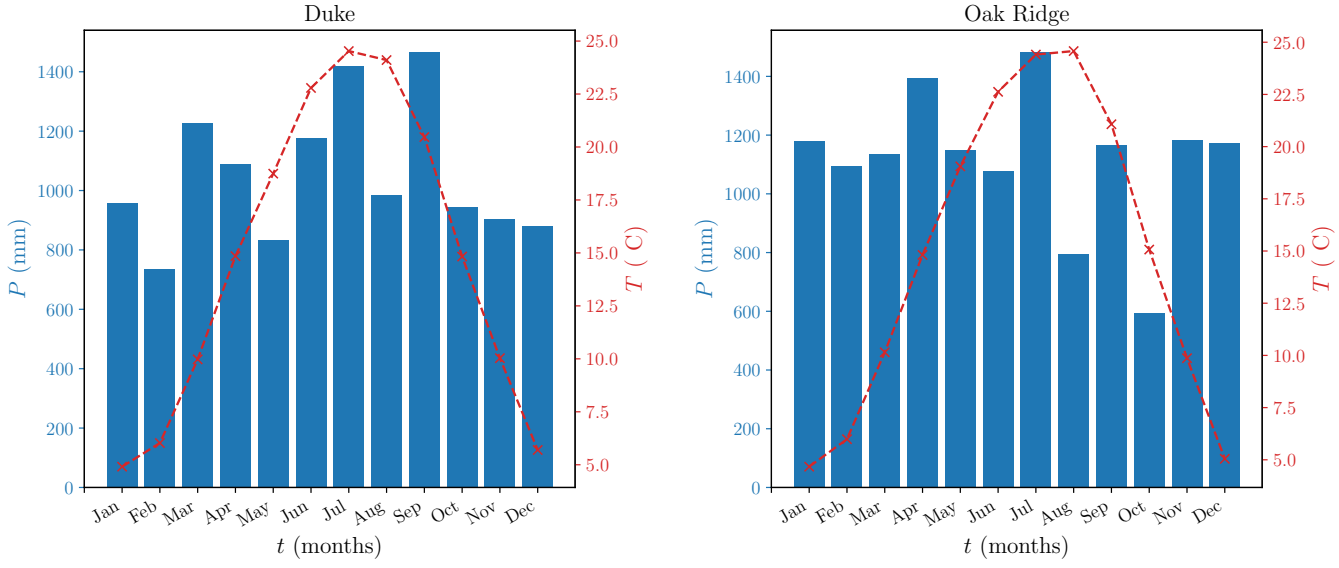

Figure 2. Mean seasonal temperature (red dashed line) and precipitation (blue bars) at both sites during the experiment period: 1996-2007 at Duke (left) and 1998-2008 at Oak Ridge (right).

For both sites, regular measurements of annual carbon fluxes, biomass pools, and soil carbon content can be found in the literature (Zaehle et al., 2014; McCarthy et al., 2010; Norby et al., 2002; Lichter et al., 2005; Jastrow et al., 2005; Johnson et al., 2004) and have been used to compare simulation results with observations.

3.2 Simulation setup and protocol

Only the dominant tree specie is modeled: pine for Duke and sweetgum for Oak Ridge. We used the corresponding ISBA PFT: temperate evergreen needle-leaved trees for Duke and temperate broadleaved deciduous trees for Oak Ridge. Initial carbon stocks are set to 0, except for the leaf and stem pools that are initialized to a minimum value. The nitrogen stock in the plant and in the soil is initialized also to an arbitrary non 0 value to support the initial photosynthesis. The same constant nitrogen deposition rate, derived from observations ($N_{\mathrm{depo}} = 1.4\ \mathrm{g_N\ m^{-2}\ y^{-1}}$; (Sparks et al., 2008; Norby et al., 2010) is prescribed at both sites. Following the protocol of Zaehle et al. (2014), the soil depth is 1 m at Duke and 2 m at Oak Ridge. The discretization is shown on the y-axis of Fig. A1. There are 8 layers at Duke and 10 at Oak Ridge. ISBA is used in offline mode, forced by meteorological forcing provided by Zaehle et al. (2014). Two sets of simulation were run: a reference simulation with only the carbon cycle referred to as the C version, and a second set with the new implementation of the nitrogen cycle called the CN version. In both C and CN versions we deactivate the pre-existing implicit N limitation parametrizations used in ISBA to down regulate the photosynthesis (Sect. 2.5 in (Delire et al., 2020)). Simulation characteristics can be found in Table 2.

For both sites and both sets of simulation, several simulation steps have been carried out in order to better represent the site and its history. The protocol is the following. First, there is a spinup. We cycled over a spinup forcing that uses meteorological

https://doi.org/10.5194/egusphere-2026-791
Preprint. Discussion started: 10 April 2026

	Duke	Oak Ridge
Coordinates	35°58' N, 79°06' W	35°54' N, 84°20' W
Forcing period	1996-2007	1998-2008
Clay fraction (%)	0.35	0.24
Sand fraction (%)	0.35	0.21
Rooting depth (m)	1	2
Soil depth (m)	1	2
Number of soil layers	8	10
Volumetric water content at wilting point	0.22	0.18
Volumetric water content at saturation	0.46	0.47

Table 2. Simulation characteristics of the two sites studied.

data of the FACE experiment with CO_2 concentration held constant at pre-industrial level. The criterion to end the spinup is discussed in the next section. Then, CO_2 concentration was gradually increased to simulate the industrial period. Historical meteorological forcing was used. This step lasted until the start of the forest plantation. At both sites, a clearing occurred before tree planting. Therefore, the biomass was reset to 0 and a simulation was run until the beginning of the FACE experiment. This step is referred to as plantation. There were 2 simulations run for the FACE experiment: one at ambient CO_2 and one at elevated CO_2. Table 3 summarizes the simulation protocol at each site.

Site	Spinup	Industrial	Plantation	FACE experiment
Duke	*	1863-1982	1983-1995	1996-2007
Oak Ridge	*	1860-1987	1988-1997	1998-2008

Table 3. Simulation steps carried out to equilibrate the model and to represent the sites history. For the spinup duration *, see Table 4

3.3 Spinup

The spinup is a critical part of the simulation process and there can be several criteria to define whether a simulation is ready to be run. Typically, spinup is considered complete when carbon pools reach a steady state, i.e., when the average total carbon stock per year stabilizes indicating system equilibrium.

A first spinup was done following this method for both sites. At Duke, equilibrium was reached after 1200 years and 2400 years for C and CN version respectively. At Oak Ridge, equilibrium was reached after 1100 and 2200 years. However, this method overestimates soil carbon content compared to field observations. For the top 15 cm of soil, observed values are 1977 $g_C\ m^{-2}$ at Duke (Lichter et al., 2005), and 2670 $g_C\ m^{-2}$ at Oak Ridge (Jastrow et al., 2005). For each set of simulation (C or CN), we compute the total below-ground litter and soil carbon in the first four soil layers to match the measurement depth. Table 4 summarizes the simulated values, which significantly exceed observed levels. However, letting the system reach

https://doi.org/10.5194/egusphere-2026-791
Preprint. Discussion started: 10 April 2026

equilibrium assumes that vegetation and soils at these sites are the result of hundreds of years of present day climate with no disturbances, which is not realistic.

An alternative approach is to stop the spinup once the soil C content reaches observed values. This method resulted in much shorter spinup durations: 21 years and 45 years for the C and CN versions respectively, at Duke; and 21 and 87 years at Oak Ridge. The first spinup type is denoted as 'eq' (equilibrium-based) and the second 'real' (observation-based) in the following sections.

	observations	spinup eq		spinup real	
		C	CN	C	CN
	carbon stocks ($g_C\ m^{-2}$)			time (years)	
Duke	1 977	9 481	9 910	21	45
Oak Ridge	2 670	13 302	13 017	21	87

Table 4. Total soil carbon (soil litter and SOC) in $g_C\ m^{-2}$ in the first soil layers as measured and after equilibrium is reached in simulations. Time in years to match observed values in the "spinup real".

Then from each spinup type, industrial, plantation and FACE experiments simulations are conducted. Figure 3 shows the impact of the spinup on the NPP results. For both sites, the C only simulations are not impacted by the type of spinup. However for the CN simulations, discrepancies are observed due to N limitations. The initial condition defines the N status in the system, a greater C soil content leads to higher mineral N pool which supplies then the labile pool. After the equilibrium spinup, the average N in the system ($N_{\text{min}} + N_{\text{labile}}$) is of 3.24 $g_N\ m^{-2}$ at Duke and of 5.72 $g_N\ m^{-2}$ at Oak Ridge. For the spinup 'real', we found a value of 1.64 $g_N\ m^{-2}$ at Duke and 3.99 $g_N\ m^{-2}$ at Oak Ridge. Note that the NPP simulated by the CN version after equilibrium spinup is very close to the one simulated by the C version, indicating that the equilibrium spinup results in a system not limited in N. We chose the type of spinup that results in a soil carbon content equal to observations. In what follows, all simulations results originate from a spinup 'real'.

4 Results

4.1 Sensitivity of Carbon and Nitrogen Fluxes to increased CO_2

We evaluate our model by comparing it to observations and multi-model simulations from Zaehle et al. (2014) who evaluated 11 models at the Duke and Oak Ridge sites. We compare our model results with the minimum, maximum and mean of these 11 models, as well as to the observational data given by Zaehle et al. (2014) (Fig. 2 and 3). Results are shown on Fig. 4 and 5.

At Duke under ambient CO_2 (Fig. 4, top left), both model versions result in annual NPPs within the 11-model range. The CN version performs better, with a smaller bias relative to observations (145 $g_C\ m^{-2}\ y^{-1}$ vs 157 for the C version) and improved interannual variability (correlation of 0.66 vs 0.64). At Oak Ridge, the C version overestimates NPP (bias of 520 $g_C\ m^{-2}\ y^{-1}$). Results of the CN version are within the 11-model range and better match observations (bias of 178 $g_C\ m^{-2}\ y^{-1}$). However,

https://doi.org/10.5194/egusphere-2026-791
Preprint. Discussion started: 10 April 2026

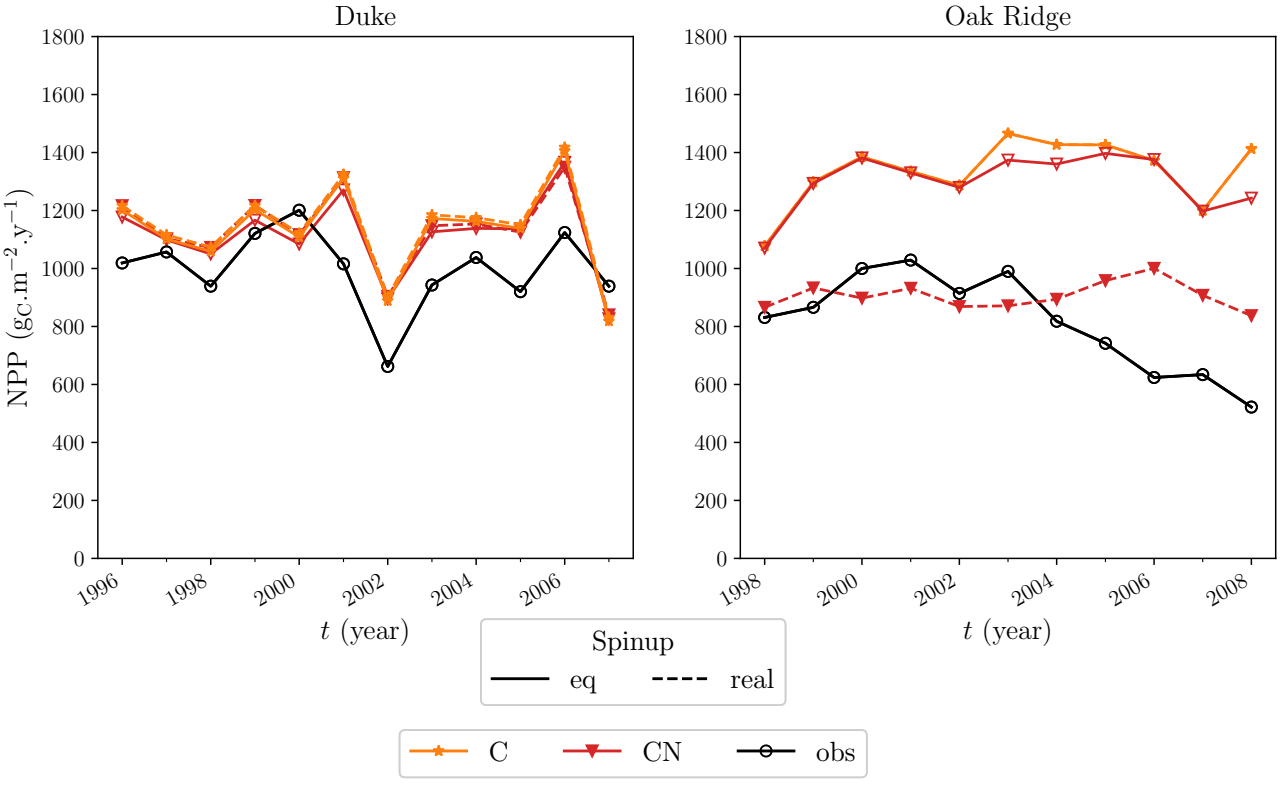

Figure 3. Simulated NPP in $g_C\ m^{-2}\ y^{-1}$ at ambient CO_2, starting from equilibrated (spinup eq, plain lines) and observation-derived soil carbon pools (spinup real, dotted lines) for Duke (left panel) and Oak Ridge (right panel). Results from C (orange stars) and CN (red triangles) simulations are compared to observations extracted from Zaehle et al. (2014) (black circles).

both model versions fail to capture the observed post-2003 decline in forest productivity associated with progressive nitrogen limitation Norby et al. (2010), resulting in weak correlations with observations. This could be explained by an overestimation of the initial inorganic N stocks as discussed by Zaehle et al. (2014). At elevated CO_2, the C-only version overestimates the NPP response at both sites (Fig. 4, bottom). Including N limitation (CN version) reduces this response. It is in better agreement with the observations at Duke (smaller bias), but the N limitation at Oak Ridge is excessive (strong negative bias). At Duke, the C version of the model accurately represents the inter-annual variability of the response, as indicated by a high correlation. The correlation decreases with the CN version. At Oak Ridge, both versions of the model yields weak correlation.

Figure 5 shows the annual N assimilation flux from soil to plant, N_{up}, which can only be analyzed with the CN version of the model. Under ambient CO_2 (top panel) N_{up} is slightly underestimated at Duke (bias of -1 $g_N\ m^{-2}\ y^{-1}$) and overestimated at Oak Ridge (bias of 7). At both sites, the model shows weak skill in reproducing the interannual variability. At Duke, the modeled CO_2 response is in good agreement with the observations and performs better than the multi-model mean. At Oak Ridge, the CO_2 response of the uptake flux is close to the multi-model mean but both fail to represent the inter annual

https://doi.org/10.5194/egusphere-2026-791
Preprint. Discussion started: 10 April 2026

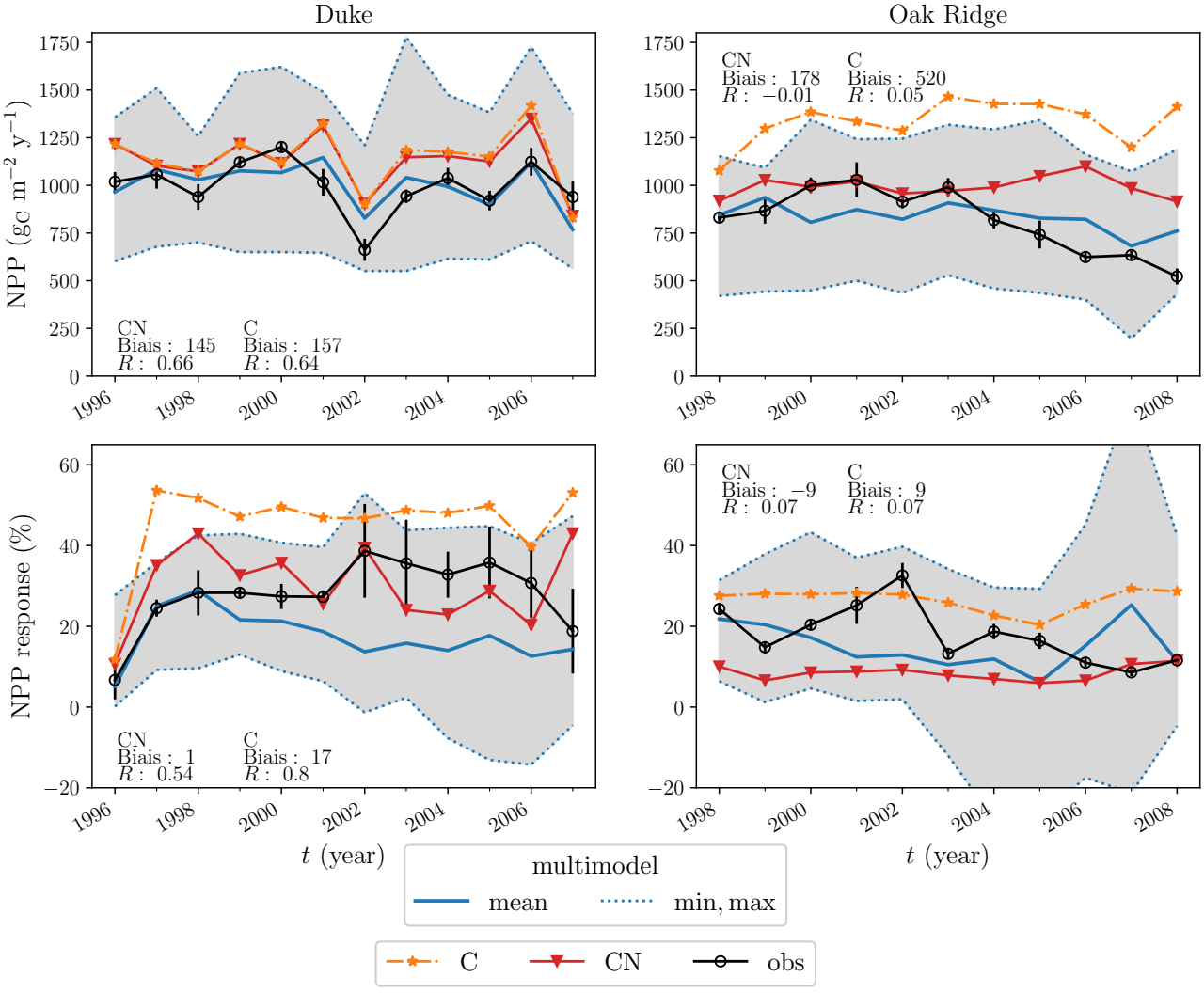

Figure 4. NPP in g_C m^{-2} y^{-1} on control plots (top panel) and response of NPP to elevated CO_2 in % (bottom). Results at Duke (left), Oak Ridge (right). Comparison of ISBA performance (C version, orange stars, and CN version, red triangles) with multi model analysis conducted by Zaehle et al. (2014) (mean blue thick line, model range: grey area delimited by dotted blue lines) and observations (black circles).

variability. On average, an increase of the uptake flux due to elevated CO_2 is observed and modeled at Duke and Oak Ridge to sustain the increase in NPP. However, the underlying process differ between sites. At Duke, SOM decomposition happened
370 faster, increasing mineralization and thus available N (Drake et al., 2011). At Oak Ridge, increased C allocation to fine roots led to greater root biomass and deeper roots allowing trees to access more N. This adaptive response is likely linked to the site history, a former agricultural land (Iversen et al., 2012). Such adaptation strategies are not represented by the model. Instead,

https://doi.org/10.5194/egusphere-2026-791
Preprint. Discussion started: 10 April 2026

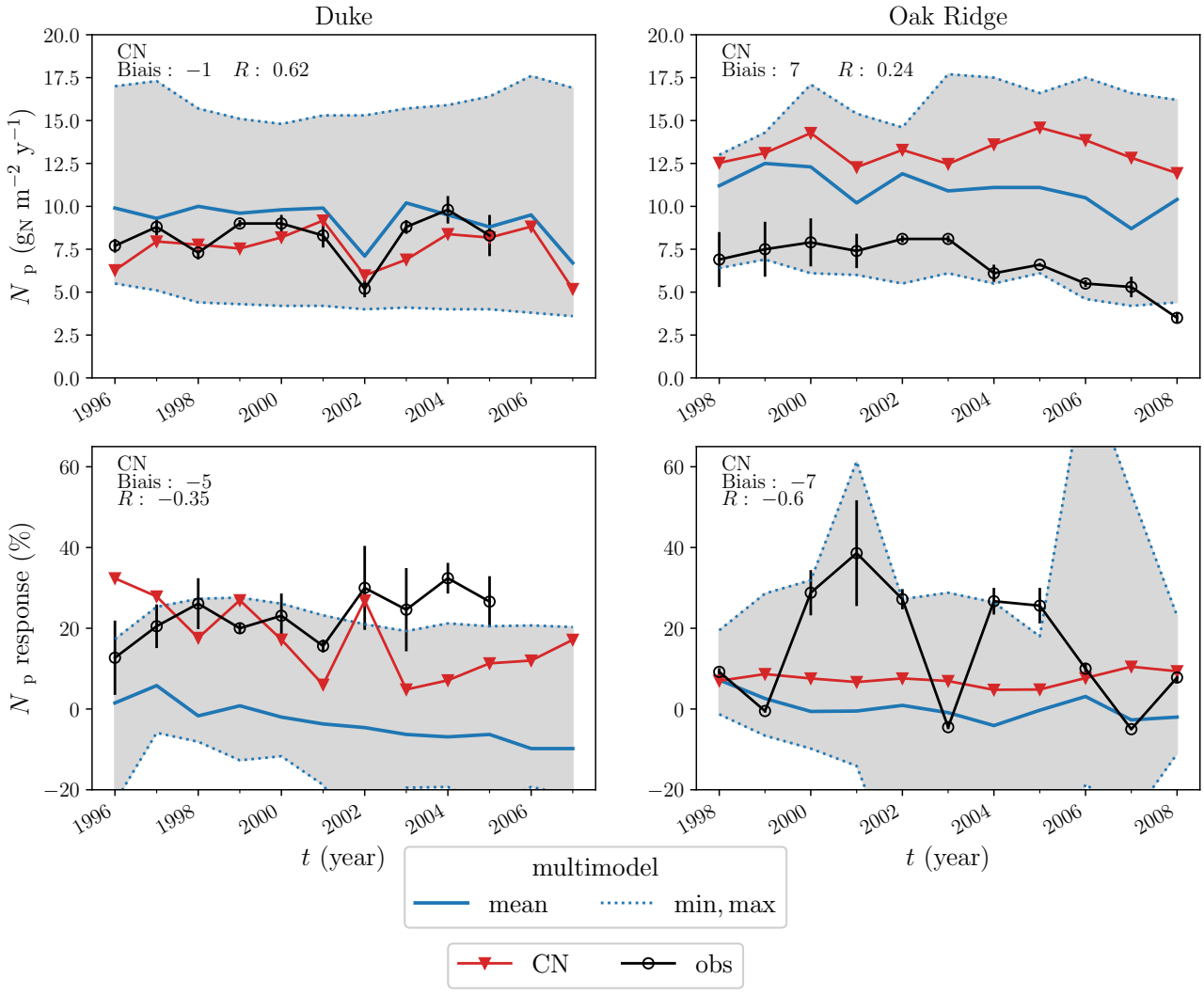

Figure 5. N_{up} in g_N m^{-2} y^{-1} on control plots (top panel) and response of N_{up} in % to elevated CO_2 (bottom). Comparison of ISBA performance (CN version, red triangles) with multi model analysis conducted by Zaehle et al. (2014) (mean blue thick line, model range: grey area delimited by dotted blue lines) and observations (black circles).

in the model, the increased N_{up} is due to increased available N in the mineral pool related to increased BNF mostly. Processes linked to the soil N dynamics are discussed in Sect. 4.3.

4.2 Vegetation and soil Carbon stocks and response to CO_2

At Duke, under ambient CO_2, the C version overestimates biomass in the woody components for the year 1997 (Table 5). This leads to an overestimation of the total biomass, although it underestimates fine-root biomass. Including the nitrogen cycle

https://doi.org/10.5194/egusphere-2026-791
Preprint. Discussion started: 10 April 2026

	Leaves (B_1)	Branches ($B_2 + B_3$)	Fine roots (B_4)	Stems (B_5)	Coarse roots (B_6)	Total biomass
obs	273	601	328	3 334	929	5 465
C	247	917	141	6 325	1 242	8 871
CN	245	907	140	6 194	1 213	8 699

Table 5. Observed biomass (McCarthy et al., 2010) vs simulated (versions C and CN) in $g_C\ m^{-2}$ for the year 1997 on ambient plots at Duke.

slightly reduces woody biomass but doesn't improve leaves and fine-root biomass. At Oak Ridge, the total biomass simulated for 1998 is 7 097 $g_C\ m^{-2}$ using the C version and 5 755 $g_C\ m^{-2}$ using the CN version. As at Duke, inclusion of the N cycle reduces C accumulation in woody biomass. No observational data are available for comparison.

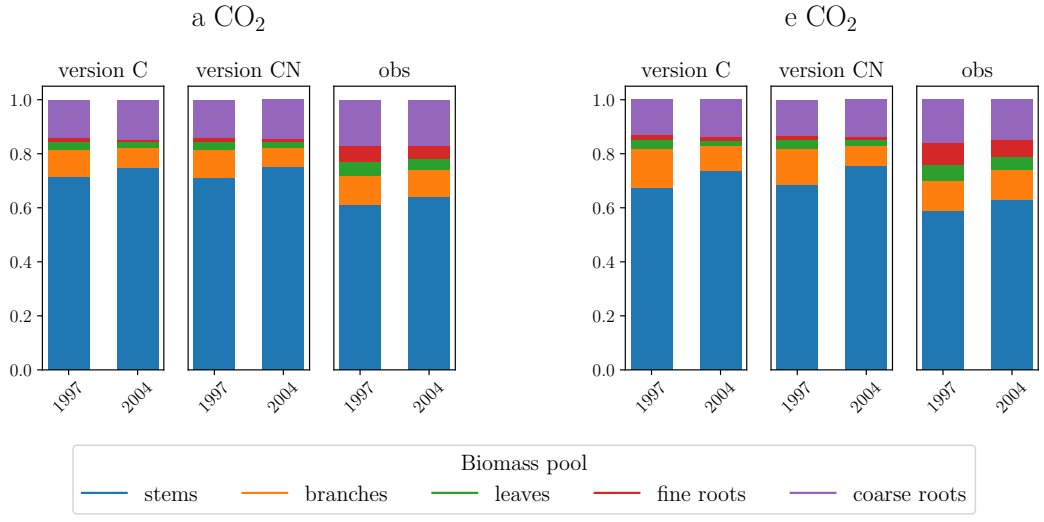

Figure 6. Partitioning of carbon in the biomass pools as a function of time at Duke. Comparison between the C (left column) and CN (middle column) model versions, and the observations (McCarthy et al., 2010) (right column),for plots under ambient (top panel) and elevated CO_2 (bottom panel).

At Duke under ambient CO_2, the carbon partitioning between biomass pools changed over time (Fig. 6) as discussed in McCarthy et al. (2010). The allocation to woody tissues increased, which is expected in an ageing forest. Both model versions reproduce this behavior, although the magnitude of the increase is smaller, and carbon allocation to wood is overestimated.

At Oak Ridge, no allocation shift was observed during the first 3 years, as indicated by biomass increments measured in 1998, 1999 and 2000 (Table 6). The proportion of C allocated to wood ($\Delta(B_2+B_3+B_5)/\Delta B_{tot}$) and fine roots ($\Delta B_4/\Delta B_{tot}$) remained constant over time. On average, 60 % of the carbon increment was stocked in wood and 12 % in fine roots. Both model versions similarly show no allocation shift during the first 3 years or over the full simulation period (1998-2008). However, the modeled proportion of carbon increments allocated to wood is higher than observed (84 % in average) while it is underestimated for fine roots (-1 % in average). Inclusion of the nitrogen cycle does not affect these results.

https://doi.org/10.5194/egusphere-2026-791
Preprint. Discussion started: 10 April 2026

	ambient CO_2			elevated CO_2		
Fine roots (B_4)						
	1998	1999	2000	1998	1999	2000
obs	81	103	104	96	133	221
C	-1	5	-13	6	12	-4
CN	-8	-5	-11	-8	2	-10
Wood ($B_2 + B_3 + B_5$)						
	1998	1999	2000	1998	1999	2000
obs	456	433	513	606	498	550
C	241	531	474	471	719	666
CN	206	403	305	317	431	349
Total biomass						
	1998	1999	2000	1998	1999	2000
obs	726	751	848	911	874	1 026
C	292	702	513	548	926	732
CN	244	534	316	359	572	363

Table 6. Increase of fine roots ΔB_4, wood $\Delta(B_2 + B_3 + B_5)$, and total biomass ΔB_{tot} for years 1998, 1999 and 2000 at Oak Ridge in $g_C\ m^{-2}\ y^{-1}$. Observations extracted from Norby et al. (2002) are compared to simulations (C and the CN versions).

Under elevated CO_2 treatment, total biomass at Duke increased by 6 204 $g_C\ m^{-2}$ between 1997 and 2004 (McCarthy et al., 2010), corresponding to a 34 % relative to ambient plots. During the same time period, the C version simulates a 74 % increase in response to elevated CO_2, whereas the CN version a 47 % increase. At Oak Ridge, between 1998 and 2008, we find a 37 % increase according to the C version and 15 % for the CN version. No data are available for comparison. Overall, the CN version limits the modeled carbon sink, which is an improvement at the Duke site. CO_2 enrichment has no effect on the partitioning of carbon in biomass at Duke (Fig. 6), a feature that is well represented by both model versions. As mentioned earlier, an increase in fine root biomass was observed at Oak Ridge (Norby et al., 2002), from 11 % in 1998 to 22 % in 2000 (Table 6). Both model versions fail to represent this shift as the model does not include a dynamic allocation scheme. The N cycle does not have an impact on the partitioning of biomass.

Soil carbon content observations are only available for the upper layers of the soil. Table 7 summarizes SOC content in the soil between 0 and 15 cm measured at Duke and Oak Ridge together with simulation results. Both the model versions overestimate the SOC content, but the addition of the nitrogen cycle improves the results.

In response to elevated CO_2, contrasting dynamics were observed at Duke and Oak Ridge. At Duke, the forest floor mass (litter and fine roots) increased under elevated CO_2, but little SOM accumulation was observed (Drake et al., 2011). Conversely, at Oak Ridge, there was no accumulation in the forest forest (Johnson et al., 2004), while SOM accumulation occurred due to increased fine root production rapidly decomposed (Iversen et al., 2012) (see Table 7, accumulation of C in the first soil layers is 3 times higher at elevated CO_2). These contrasting dynamics in SOC and forest floor are not well represented by the model.

https://doi.org/10.5194/egusphere-2026-791
Preprint. Discussion started: 10 April 2026

	Duke			Oak Ridge	
	ambient	elevated		ambient	elevated
C					
1996	5 896	5 896	1997	9 140	9 140
2002	5 761	6 044	2002	8 840	9 009
Δ	-135	148	Δ	-300	-131
CN					
1996	5 136	5 135	1997	5 494	5 494
2002	5 149	5 328	2002	5 571	5 585
Δ	14	193	Δ	77	91
obs					
1996	1 977	2 142	1 997	2 670	2 793
2002	2 407	2 734	2002	2 732	2 994
Δ	430	592	Δ	62	201

Table 7. Simulated vs observed carbon content in soil between 0 and 15 cm in 2002 in $g_C\ m^{-2}$. Simulations are from C and CN versions. C content is computed as the sum of soil litter C and SOC on the first 4 layers. Observations data are extracted from Lichter et al. (2005) for Duke and Jastrow et al. (2005) for Oak Ridge.

There is an increase in SOC content modeled in response to elevated CO_2 at both sites. This accumulation is stronger at Duke than at Oak Ridge. The C version models an increase in SOC accumulation of 210 % at Duke and 56 % at Oak Ridge while the CN version results in 1 279 % increase at Duke and 18 % at Oak Ridge. Both model versions simulate an increase of C in the forest floor (computed as surface litter L_{surf} and fine-roots B_4) in response to elevated CO_2 at both sites. The increase is smaller with the CN version.

This study points out the limitations of the carbon cycle model in ISBA. The allocation pattern is not flexible, therefore adaptions to environmental changes cannot be captured. This impacts carbon partitioning within the soil and the representation of decomposition processes. Vertical soil discretization is important to improve the modeling of C and N dynamics (Norby et al., 2010; Iversen et al., 2012; Zaehle et al., 2014). However this is not sufficient to represent the response to elevated CO_2 as shown here. Other processes are lacking such as a dynamical root profile or the effect of microbial communities (Drake et al., 2011).

4.3 Modeled N dynamics

https://doi.org/10.5194/egusphere-2026-791
Preprint. Discussion started: 10 April 2026

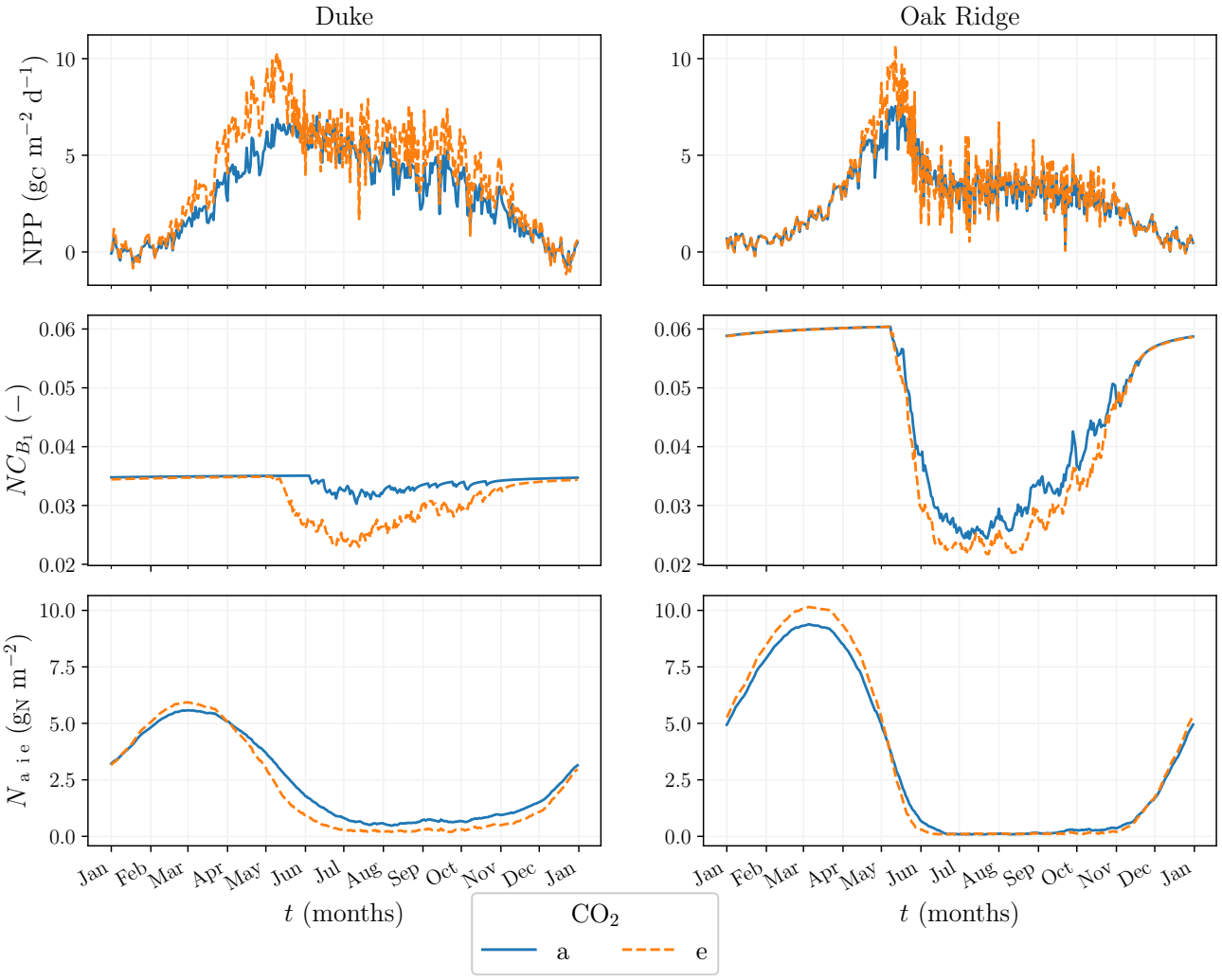

Figure 7. Average seasonal cycle of NPP, NC_{B_1}, and N_{labile} at Duke (left) and Oak ridge (right) with the CN model version at ambient CO_2 (blue plain lines) and elevated CO_2 (orange dashed lines).

This section focuses on the CN version of the model to evaluate the new implementation. Figure 7 shows the dynamics of nitrogen in the vegetation and Fig. 8 its dynamics as bulk in the soil. The vegetation labile pool and the soil mineral pool are coupled through the uptake flux (shown in Fig. 8) that determines N availability for plant growth. In early spring, photosynthesis is mainly sustained by the labile pool. Progressively, when the labile pool empties around April or May, the N/C ratio of leaves starts to decrease. This triggers an increase in uptake flux that is able to sustain NPP through the summer. Figure 7 shows

https://doi.org/10.5194/egusphere-2026-791
Preprint. Discussion started: 10 April 2026

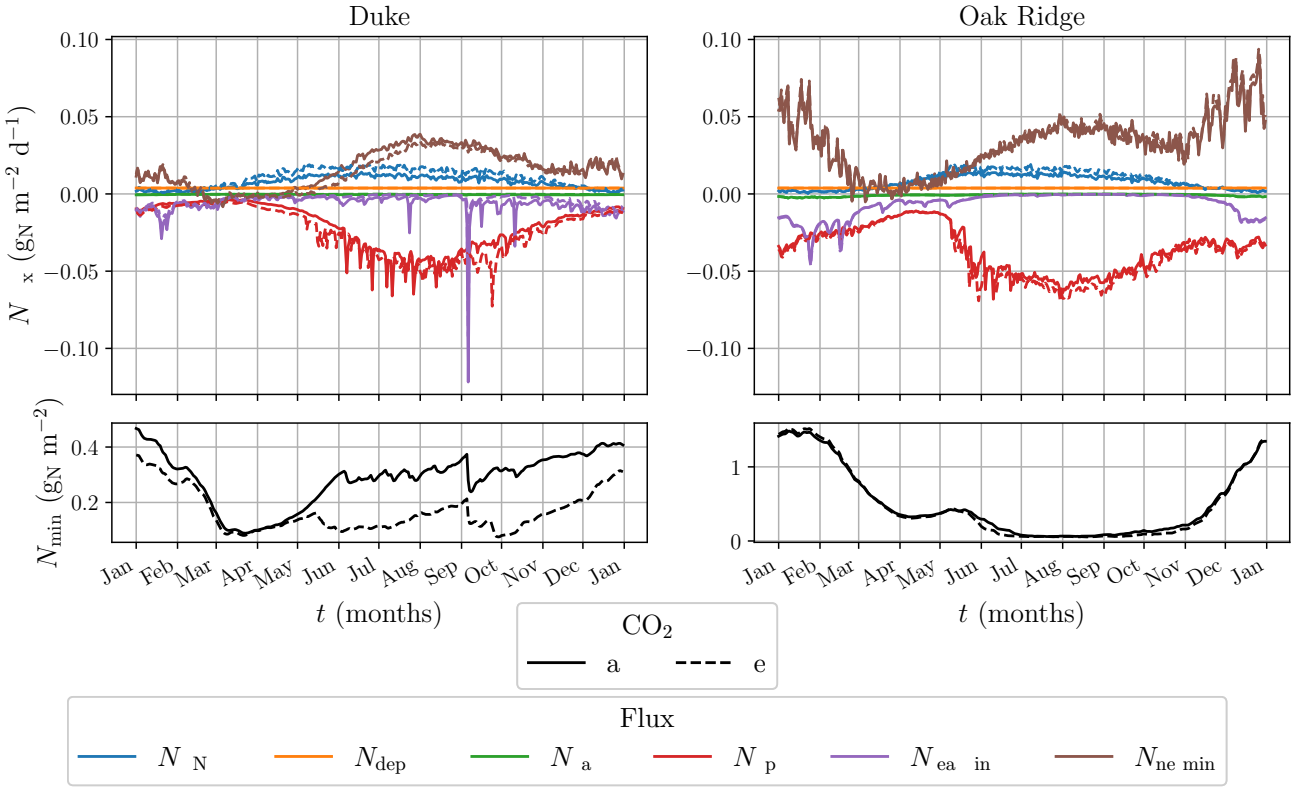

Figure 8. Average seasonal cycle of the simulated bulk mineral N pool (bottom) and its input and output fluxes (top), at Duke (left) and Oak Ridge (right), at ambient (plain line) and elevated CO_2 (dashed line). Input fluxes are positive, output fluxes negative. Pool content is shown in g_N m^{-2} and fluxes are in g_N m^{-2} d^{-1}.

	Duke			Oak ridge		
	ambient CO_2	elevated CO_2	Response (%)	ambient CO_2	elevated CO_2	Response (%)
N_{BNF}	2.67	3.83	44	2.73	3.36	23
N_{depo}	1.39	1.39	0	1.39	1.39	0
N_{up}	7.53	8.78	17	13.16	14.13	7
N_{gas}	0.156	0.087	-44	0.294	0.287	-3
$N_{leaching}$	2.33	1.48	-36	2.41	2.44	2
N_{netmin}	5.91	5.11	-14	11.68	12.05	3

Table 8. Annual input and output fluxes that contribute to the mineral nitrogen dynamics. Fluxes are in g_N m^{-2} y^{-1}.

that the N/C ratio evolves as a function of the nitrogen demand. The ratio decreases as the labile pool is depleted. There is no observation to compare this results with, but the model behaves as expected.

https://doi.org/10.5194/egusphere-2026-791
Preprint. Discussion started: 10 April 2026

The main source of mineral N at Duke and at Oak Ridge is net mineralization. BNF is of the same order of magnitude at both sites (see Table 8), which is consistent with the similar magnitude of NPP at the two sites, as BNF is proportional to NPP. A new global BNF estimates suggests that the BNF rate used in this study overestimates this flux (Reis Ely et al., 2025). As N_{BNF} varies with NPP, it peaks in summer. N_{depo} is prescribed and identical at both sites. Net mineralization however is twice as high at Oak Ridge as at Duke, especially in winter. As a result, the mineral N pool is larger at Oak Ridge for most of the year. This drives soil N dynamics, as all output fluxes are proportional to N_{min}. N_{leaching}, N_{gas}, and N_{up} are hence greater at Oak Ridge.

Few measurements are available for comparison. At Duke, Johnson et al. (2004) measured in 1998 on ambient plots an annual N_2O flux of 0.0070 $g_N\ m^{-2}\ y^{-1}$, and an annual leaching flux <0.001 $g_N\ m^{-2}\ y^{-1}$. For the same year, the model simulates an N_2O flux that is twice as high (0.0162 $g_N\ m^{-2}\ y^{-1}$) and overestimates by several orders of magnitude the leaching flux (3.39 $g_N\ m^{-2}\ y^{-1}$). Reasons for this higher leaching are related to the vertical profile of the soil discussed further down. Calibration of the gaseous outputs is difficult due to the limited number of observations available at these sites and will be studied in the future on agricultural surfaces where more N_2O data are available.

To better understand the dynamics of the net mineralization flux, Figure 9 depicts the mineralization and immobilization fluxes. Mineralization due to respiration of SOC pools, F_{SOC}, dominates the net mineralization flux at both sites (purple line). The mean annual amount of carbon decomposition is higher at Duke than Oak Ridge, as indicated by heterotrophic respiration rates of 357 $g_C\ m^{-2}\ y^{-1}$ at Duke and 324 $g_C\ m^{-2}\ y^{-1}$ at Oak Ridge. This results in higher F_{SOC} at Duke. Inputs from surface biomass, $F_{B_x,L_{\mathrm{surf}}}$ result from the balance between the N/C ratio of biomass and that of surface litter. This balance is controlled by the N/C ratio of leaves, the only one flexible. Therefore $F_{B_x,L_{\mathrm{surf}}}$ is greater during winter, when nitrogen demand is low and leaf N/C ratio is high. This leads to an accumulation of nitrogen near the soil surface as exhibited by Fig. A2 and A3. $F_{B_x,L_{\mathrm{surf}}}$ and, to a lesser extent, $F_{B_x,L_{\mathrm{soil}}}$, are greater at Oak Ridge because the imposed N/C ratios of biomass pools in broadleaf deciduous trees are higher than those of needleleaf evergreen trees (Table B1). Although annual biomass turnover is greater at Duke (688 $g_C\ m^{-2}\ y^{-1}$) than at Oak Ridge (615 $g_C\ m^{-2}\ y^{-1}$), the higher N/C ratios of biomass pools at Oak Ridge result in greater N release at that site. Around March at Duke, net mineralization is dominated by immobilization associated with surface litter decomposition that depletes the mineral pool (Fig. A2). The immobilization flux from litter decomposition is stronger at Duke, again due to the lower N/C ratios.

As mentioned in Sect. 2.6, the current version of the model does not represent the vertical movement of N in the soil. Therefore, to avoid unrealistic accumulation of N, we imposed a vertical profile of some input and output fluxes along the soil depth. N resulting from N deposition for instance would otherwise accumulate in the upper layer of the soil. Both N_{BNF} and N_{depo} are distributed according to the soil water profile (eq. 12 and Fig. A1). Therefore, deeper soil layers are more enriched in N because they contain more water (Fig. A2 and A3). This is a model artifact that will be addressed in a future version of the model through an explicit representation of vertical nitrogen transport in the soil. The imposed vertical profiles of gas loss and leaching follow the vertical profile of mineral N in the soil. N uptake follows the root profile and is proportional to mineral N. Because net mineralization provides a high supply of N near the soil surface, uptake fluxe is greatest in the upper soil layers.

https://doi.org/10.5194/egusphere-2026-791
Preprint. Discussion started: 10 April 2026

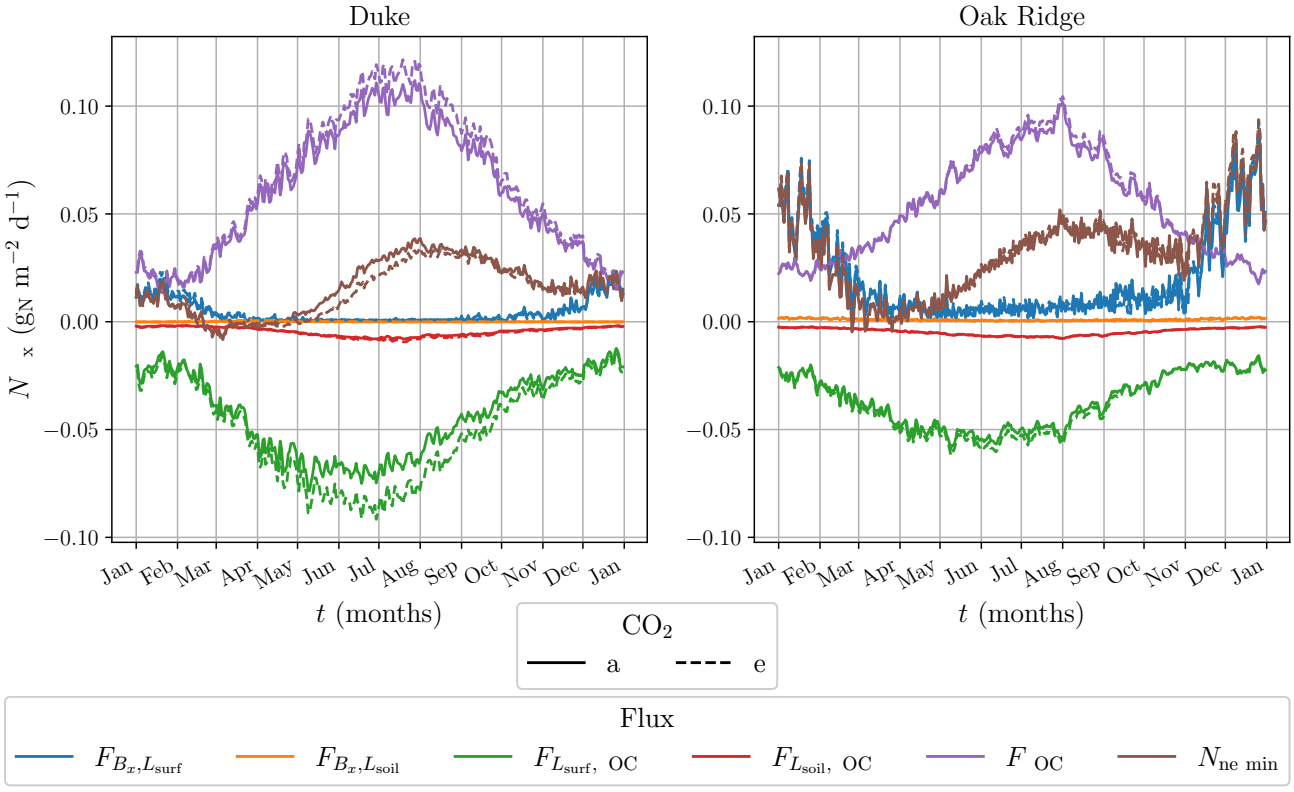

Figure 9. Climatology of the simulated mineralization and immobilization fluxes as well as the net mineralization flux. Fluxes are in g_N m^{-2} d^{-1}. Results for Duke are on the right panel and for Oak ridge on the left. Results are shows for plots at ambient and elevated CO_2.

In response to elevated CO_2, the BNF which is strongly tight to the NPP, is enhanced on both sites. At Duke, the increase of litter enhances the immobilization flux, thereby reducing net mineralization, whereas at Oak Ridge, there is little change in net mineralization. This is not coherent with observations: the increase in forest floor at Duke stimulated microbial activity, accelerating SOM decomposition and mineralization, thereby increasing N availability (Drake et al., 2011). At Oak Ridge, it is the increase in fine roots that increased the SOC content due to fast root turnover, leading to higher immobilization and reduced N availability (Iversen et al., 2012). These discrepancies originate from differences in the simulated soil carbon dynamics. Moreover, measurements show that N/C ratios are important parameters that control the net mineralization flux. Plants can adapt to N shortage by decreasing their N/C ratio. This dampens N-limitation effects but affects the litter quality: immobilization is increased resulting in less N available (Finzi et al., 2006). However implementing flexible N/C ratios in models is not straightforward as identified by Zaehle et al. (2014) multi model analysis. Without appropriate constraints, such flexibility can lead to unrealistic stoichiometric ratios (Zaehle et al., 2014).

https://doi.org/10.5194/egusphere-2026-791
Preprint. Discussion started: 10 April 2026

In the simulations, the main source of new N is the BNF, proportional to NPP that increases under elevated CO_2 conditions. The newly available N is used by plants (increase of N_{up}). BNF is an important external source of nitrogen and can alleviate the N limitation (Liang et al., 2016). However, external nitrogen inputs (mostly ammonia) are known to directly regulate BNF activity in cells (Dixon and Kahn, 2004), as well as in diverse soil and forest organism (e.g., Ackermann et al. (2012) in moss soil carpet, Darnajoux et al. (2022) in coastal sediment). The current parametrization as a function of NPP, does not take into account the N status of the soil. Moreover, it makes BNF dependent on the NPP response to CO_2. This could be challenged by implementing a more process-based parametrization of BNF (Thomas et al., 2015; Kou-Giesbrecht and Arora, 2022).

5 Conclusions

In this study, we document the development of the nitrogen cycle in ISBA, the land surface component of the CNRM ESM. The model is evaluated at two FACE experiment sites: Duke and Oak Ridge. We compare the performance of the C (reference version) with that of the CN version that uses the newly implemented N cycle.

Comparison with the multi-model analysis carried out by Zaehle et al. (2014) shows that the CN version reduces several biases present in the C version of the model. Simulations performed with the new version are in the multi-model range, and the response to elevated CO_2 is closer to observations.

The C version of ISBA overestimates the carbon stocks at both sites. The new implementation improves the results, as nitrogen limitations constrain photosynthesis, resulting in less carbon entering the system. All carbon pools are reduced when the nitrogen cycle is added. Although the model does not capture site-specific adaptative responses, such as allocation shifts or microbial activity, it does accurately depict the main features of the response to elevated CO_2. Carbon storage increases under elevated CO_2, but this carbon sink is substantially reduced when nitrogen cycle processes are taken into account.

The N dynamics reproduce the main expected features. However, biases from the C dynamics of ISBA are propagated to the coupled C-N dynamics. This could be addressed by implementing flexible N/C ratios, constraints on the allocation patterns or an evolving root profile. While the model does not capture site-specific adaptative strategies, its overall performance is encouraging. Further improvements could include an explicit representation of vertical mineral nitrogen dynamics and a more process-based parameterization of BNF.

Code and data availability. ISBA is part of the software SURFEX from the CNRM open-source website https://opensource.umr-cnrm.fr under the CeCILL-C license. The version including the nitrogen cycle is available via Zenodo at https://doi.org/10.5281/zenodo.18459080 (Decayeux, 2026). Data used for the figures are also provided on the Zenodo deposit.

Appendix A: Carbon dynamics

ISBA represents the vegetation by six biomass pools:

https://doi.org/10.5194/egusphere-2026-791
Preprint. Discussion started: 10 April 2026

- B_1, leaves
- B_2, a structural pool representing stems in the case of grass and crop, and new twigs for trees
- B_3 for numerical stability
- B_4 fine roots and root sapwood
- B_5 aboveground woody biomass (trunk and branches)
- B_6 belowground woody biomass (root heartwood)

Herbaceous plants are described by the 4 first pools while trees by the 6 biomass pools. The assimilated carbon is first allocated to the leaves. It is then reallocated to the other biomass pools using different empirical allometric relations (Gibelin et al., 2008). The dynamics of the biomass pools is described by the following equation:

$$\frac{\mathrm{d}B_x}{\mathrm{d}t} = A_x(t) - M_x(t) - S_x(t) - R_x(t),\ x \in \{1,2,3,4,5,6\} \tag{A1}$$

where A_x is the incoming flux of carbon, M_x the mortality computed as a turnover, S_x the carbon that is transferred to the other pools and R_x the respiration. For leaf biomass (B_1), A_1 is the carbon assimilated by photosynthesis. For the 5 other pools, A_x is the C reallocated from the other pools ($S_{y\neq x}$). Mortality and storage are computed from a decline term D_x:

$$D_x = B_x\left(1 - \exp\left(\frac{\Delta t}{\tau_x}\right)\right) \tag{A2}$$

where τ_x is a characteristic time depending of the pool. This quantity is then divided into mortality and storage. Biomass dynamics is computed once a day.

The litter and soil carbon dynamics follow the CENTURY model (Parton et al., 1988). There are two aboveground litter pools: a structural, C_1 and and a metabolic C_2. The dynamics is described by:

$$\frac{\partial C_i}{\partial t} = T_i + \sum_{j\neq i}(1-r_j)f_{ij}F^j_{\mathrm{oxic}} - F^i_{\mathrm{oxic}},\ (i,j) \in [1,2] \tag{A3}$$

In the soil, the dynamics is modified by Morel et al. (2019) to represent anoxic decomposition and methane-related processes. There are for each layer l two belowground litter pools: structural, C_3 and metabolic C_4, and 3 soil organic carbon pools: an active (C_5), a slow (C_6) and a passive (C_7) carbon pool, which differs from their turnover times. The equation is the following:

$$\frac{\partial C_i(z)}{\partial t} = \frac{\partial}{\partial z}\left[D(z)\frac{\partial C_i(z)}{\partial z}\right] + \frac{\partial AC_i(z)}{\partial z} + T_i(z) + \sum_{j\neq i}(1-r_j)f_{ij}F^j_{\mathrm{oxic}}(z) - F^i_{\mathrm{oxic}}(z) - r_{\mathrm{MG},i}(z)\frac{M_{\mathrm{C}}}{M_{\mathrm{CH4}}},(i,j) \in [3,7] \tag{A4}$$

F^i_{oxic} is the quantity of carbon decomposed in the pool i, a fraction r_i of this is lost as respiration. The remaining decomposed carbon, $(1-r_i)F^i_{\mathrm{oxic}}$, is divided to the other carbon pools j according a fraction f_{ij} that is a function of the soil composition

https://doi.org/10.5194/egusphere-2026-791
Preprint. Discussion started: 10 April 2026

and lignin content for litter pools. The surface litter and soil carbon dynamics is computed at the model timestep. In both equations, T_i is computed from the mortality of biomass pools as:

$$T_i = \begin{cases} \sum_{x=1,2,3,5} M_x f_{x,i}, \text{ for } i = 1,2 \\ \sum_{x=4,6} M_x f_{x,i}, \text{ for } i = 3,4 \\ 0, \text{ for } i = 5,6,7 \end{cases} \tag{A5}$$

where $f_{x,i}$ is the factor to partition turnover in structural and metabolic.

Appendix B: N/C ratio

Biomass			Litter			Soil organic carbon		
	TEBD	TENE		TEBD	TENE		TEBD	TENE
B_1	1/25	1/52	C_1, C_3	1/70	1/70	C_5	1/15	1/15
B_2	1/40	1/100	C_2, C_4	1/300	1/600	C_6	1/15	1/15
B_3	1/40	1/100				C_7	1/15	1/15
B_4	1/50	1/120						
B_5	1/200	1/400						
B_6	1/200	1/400						

PFT	$NC_{B_1,\min}$	$NC_{B_1,\max}$
TEBD	1/65	1/16
TENE	1/75	1/28

Table B1. N/C stoichiometric ratio in $g_N\ g_C^{-1}$ used in ISBA for the two PFT on which the model is tested: TEmperate Broadleaf Deciduous (TEBD) and TEmperate Needleleaf Evergreen (TENE). Left: N/C ratio for each pool. Right: Maximum and minimum values accepted for the varying N/C stoichiometric ratio of leaves (biomass pool B_1).

Appendix C: Soil nitrogen functions and parameters

C1 Nitrification

The temperature function for nitrification is described by equation C1 taken from the QUINCY model (Thum et al., 2019). Parameters used in the equation are given in Table C1.

$$f(T_l) = E_{\text{d,nit}} \frac{\exp(\frac{E_{\text{a,nit}}}{R} \frac{T_l - T_{\text{opt,nit}}}{T_l \times T_{\text{opt,nit}}})}{E_{\text{d,nit}} - E_{\text{a,nit}} \times (1 - \exp(\frac{E_{\text{a,nit}}}{R} \frac{T_l - T_{\text{opt,nit}}}{T_l \times T_{\text{opt,nit}}})} \tag{C1}$$

where T_l is the soil temperature in layer l in Kelvin. Nitrification increases as temperature rises. The soil moisture function for nitrification is described by equation C2, which models the moisture dependency with an optimum soil moisture according to

https://doi.org/10.5194/egusphere-2026-791
Preprint. Discussion started: 10 April 2026

Li et al. (2000). There is a moderate effect of moisture but nitrification is slowed if the soil is saturated. Parameters used in the equation are given Table C1.

$$f(\theta_l) = f_{\max}\theta_l^2\,(1-\theta_l)^{0.5} \tag{C2}$$

where $\theta_l = \min\left(0, \frac{w_{\mathrm{g},l}-w_{\mathrm{wilt},l}}{w_{\mathrm{sat},l}-w_{\mathrm{wilt},l}}\right)$, $w_{\mathrm{g},l}$ denotes soil water content in $\mathrm{m}^3\ \mathrm{m}^{-3}$, $w_{\mathrm{sat},l}$ the soil porosity in $\mathrm{m}^3\ \mathrm{m}^{-3}$, $w_{\mathrm{wilt},l}$ the wilting point in $\mathrm{m}^3\ \mathrm{m}^{-3}$, and $f_{\max} = \frac{25\sqrt{5}}{16}$ ensures that the function has a maximum value of 1. The parametrization follows experimental observations by Khalil et al. (2004); Ingwersen et al. (1999) and modeling works by Li et al. (1992); Parton et al. (1996); Li et al. (2000); Xu-Ri and Prentice (2008); Thum et al. (2019); Yang et al. (2009); Sulman et al. (2019).

C2 Denitrification

The temperature function is taken from the QUINCY model Thum et al. (2019). Denitrification is increasing with temperature as described by:

$$f(T_l) = \exp\left(-\frac{E_{\mathrm{a,denit}}}{R}\left(\frac{1}{T_l}-\frac{1}{T_{\mathrm{ref}}}\right)\right) \tag{C3}$$

The parameters are given in the following Table C1

Symbol	Value	Units	Reference
$E_{\mathrm{d,nit}}$	200000	$\mathrm{J\cdot mol^{-1}}$	Thum et al. (2019)
$E_{\mathrm{a,nit}}$	80000	$\mathrm{J\cdot mol^{-1}}$	Thum et al. (2019)
R	8.314	$\mathrm{J\cdot mol^{-1}\cdot K^{-1}}$	gas constant
$T_{\mathrm{opt,nit}}$	311.15	K	Thum et al. (2019)
T_{ref}	323.15	K	this study
$E_{\mathrm{a,denit}}$	47000	$\mathrm{J\cdot mol^{-1}}$	Thum et al. (2019)

Table C1. Parameters used to describe nitrification and denitrification

Appendix D: Nitrogen associated to turnover and decomposition fluxes

D1 Turnover flux from biomass pools to litter pools

The N turnover flux is computed by applying an effective N/C ratio: $NC_{\mathrm{eff},B_x} = NC_{B_x}\,(1-f_{\mathrm{trans},x})\,f_{\mathrm{corr}}$. This takes into account the retranslocation, see Sect. 2.3. The resultant nitrogen flux is obtained by comparing the input flux to what the receiving pool needs. Surface litter is supplied by the turnover of the aboveground biomass pools (1, 2, 3 and 5) and the flux is given by equation (D1). Soil litter is supplied by the biomass pools 4 and 6 (root pools), equation (D2).

$$F_{B,L_{\mathrm{surf}}} = \sum_{x=1,2,3,5} f_{x,1}M_x(NC_{\mathrm{eff},B_x}-NC_{C_1}) + f_{x,2}M_x(NC_{\mathrm{eff},B_x}-NC_{C_2}) \tag{D1}$$

https://doi.org/10.5194/egusphere-2026-791
Preprint. Discussion started: 10 April 2026

$$F_{B,L_{\text{soil}}} = \sum_{x=4,6} f_{x,3} M_x (NC_{\text{eff},B_x} - NC_{C_3}) + f_{x,4} M_x (NC_{\text{eff},B_x} - NC_{C_4}) \tag{D2}$$

D2 Flux between litter pools and SOC pools

Decomposition from the metabolic aboveground litter pool, denoted F^1_{oxic}, enters the first layer of the active SOC pool (C_5) and releases CO_2 as respiration. Decomposition from the structural surface litter pool, F^2_{oxic}, is divided in a fraction that contains lignin L_2 and goes into the slow SOC pool (C_6), a fraction with no lignin $(1 - L_2)$ that flows into the active SOC pool (C_5) and a fraction that goes to respiration.

$$\begin{aligned} F_{L_{\text{surf}},\text{SOC}} =& L_2 (NC_{C_2} - NC_{C_6}) F^2_{\text{oxic}} f_{2,6} + (1 - L_2)(NC_{C_2} - NC_{C_5}) F^2_{\text{oxic}} f_{2,5} + (NC_{C_1} - NC_{C_5}) F^1_{\text{oxic}} f_{1,5} \\ &+ \underbrace{[(1 - L_2)(1 - f_{2,5}) + L_2 (1 - f_{2,6})] F^2_{\text{oxic}} NC_{C_2} + (1 - f_{1,5}) F^1_{\text{oxic}} NC_{C_1}}_{\text{respiration}} \end{aligned} \tag{D3}$$

The decomposition of the belowground litter follows a similar path. The structural pools C_4 are decomposed into active and slow SOC pools depending on their lignin content (L_4) and the metabolic pools enter the active SOC. The resulting N flux per layer is:

$$\begin{aligned} F_{L_{\text{soil}},\text{SOC},l} =& L_{4,l} (NC_{C_4} - NC_{C_6}) F^4_{\text{oxic},l} f_{4,6} + (1 - L_{4,l})(NC_{C_4} - NC_{C_5}) F^4_{\text{oxic},l} f_{4,5} + (NC_{C_3} - NC_{C_5}) F^3_{\text{oxic},l} f_{3,5} \\ &+ \underbrace{[(1 - L_{4,l})(1 - f_{4,5}) + L_{4,l} (1 - f_{4,6})] F^4_{\text{oxic},l} NC_{C_4} + (1 - f_{3,5}) F^3_{\text{oxic},l} NC_{C_3}}_{\text{respiration}} \end{aligned} \tag{D4}$$

D3 Flux between SOC pools

Decomposition of organic carbon within the active, slow and passive pools results in a N flux of:

$$\begin{aligned} F_{\text{SOC},l} =& (NC_{C_5} - NC_{C_6}) F^5_{\text{oxic},l} f_{5,6} + (NC_{C_5} - NC_{C_7}) F^5_{\text{oxic},l} f_{5,7} \\ &+ (NC_{C_6} - NC_{C_5}) F^6_{\text{oxic},l} f_{6,5} + (NC_{C_6} - NC_{C_7}) F^6_{\text{oxic},l} f_{6,7} \\ &+ (NC_{C_7} - NC_{C_5}) F^7_{\text{oxic},l} f_{7,5} \\ &+ \underbrace{(1 - f_{5,6} - f_{5,7}) F^5_{\text{oxic},l} NC_{C_5} + (1 - f_{6,5} - f_{6,7}) F^6_{\text{oxic},l} NC_{C_6} + (1 - f_{7,5}) F^7_{\text{oxic},l} NC_{C_7}}_{\text{respiration}} \end{aligned} \tag{D5}$$

Appendix E: List of added variables

https://doi.org/10.5194/egusphere-2026-791
Preprint. Discussion started: 10 April 2026

Symbols	Units	Description
N_{labile}	$\mathrm{g_N\ m^{-2}}$	Labile nitrogen
N_{upday}	$\mathrm{g_N\ m^{-2}\ d^{-1}}$	Daily nitrogen uptake from mineral N
N_{demand}	$\mathrm{g_N\ m^{-2}\ d^{-1}}$	Nitrogen demand from biomass to meet carbon assimilation
N_{turn}	$\mathrm{g_N\ m^{-2}\ d^{-1}}$	Nitrogen turnover
N_{min}	$\mathrm{g_N\ m^{-2}}$	Mineral nitrogen ($\mathrm{NH_4^+}$ and $\mathrm{NO_3^-}$)
N_{BNF}	$\mathrm{g_N\ m^{-2}\ s^{-1}}$	Input N flux from BNF
N_{depo}	$\mathrm{g_N\ m^{-2}\ s^{-1}}$	Input N flux from deposition
N_{nit}	$\mathrm{g_N\ m^{-2}\ s^{-1}}$	Nitrification flux
N_{denit}	$\mathrm{g_N\ m^{-2}\ s^{-1}}$	Denitrification flux
N_{gas}	$\mathrm{g_N\ m^{-2}\ s^{-1}}$	Gas output from mineral pool
N_{up}	$\mathrm{g_N\ m^{-2}\ s^{-1}}$	Nitrogen uptake from mineral N
$f_{\mathrm{water},l}$	unitless	fraction of water in layer l
N_{leaching}	$\mathrm{g_N\ m^{-2}\ s^{-1}}$	N leaching flux

Table E1. Variables added for the nitrogen cycle.

https://doi.org/10.5194/egusphere-2026-791
Preprint. Discussion started: 10 April 2026

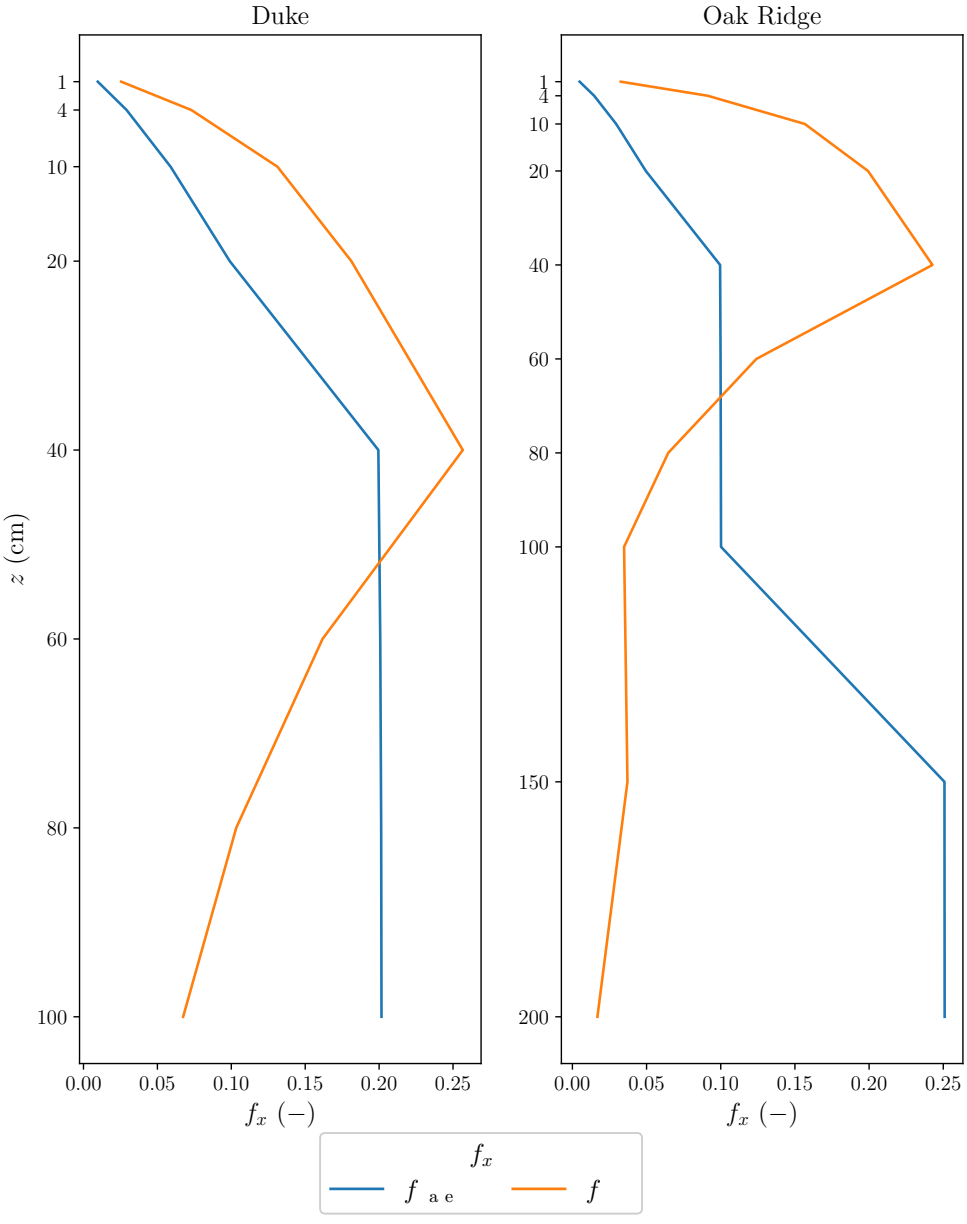

Figure A1. Water profile (blue) and root profile (orange) at Duke (left) and at Oak Ridge (right). The y-axis gives the vertical discretization of the soil, by indicating the depth of each layer.

https://doi.org/10.5194/egusphere-2026-791
Preprint. Discussion started: 10 April 2026

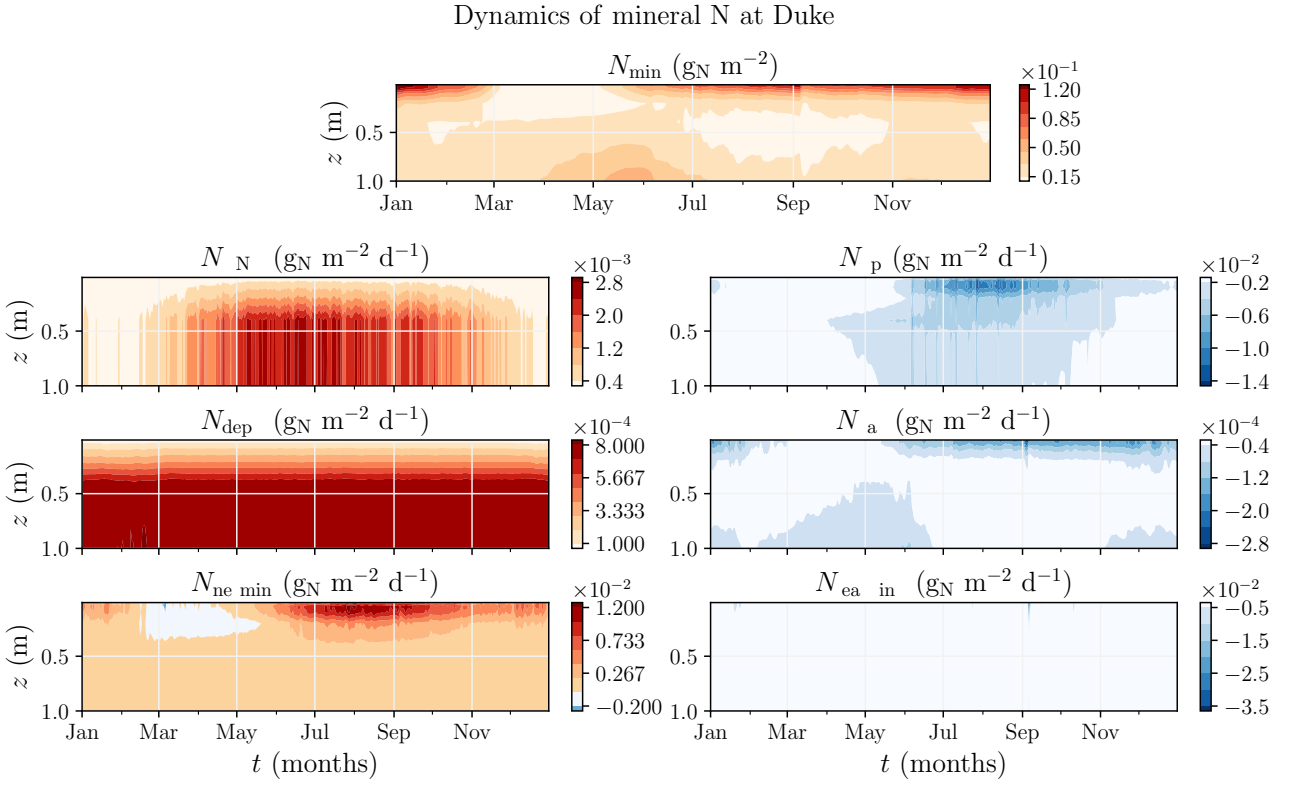

Figure A2. Seasonal cycle of the vertical soil profile of N fluxes and mineral pool at Duke for the reference plot exposed to ambient CO_2 concentration.

https://doi.org/10.5194/egusphere-2026-791
Preprint. Discussion started: 10 April 2026

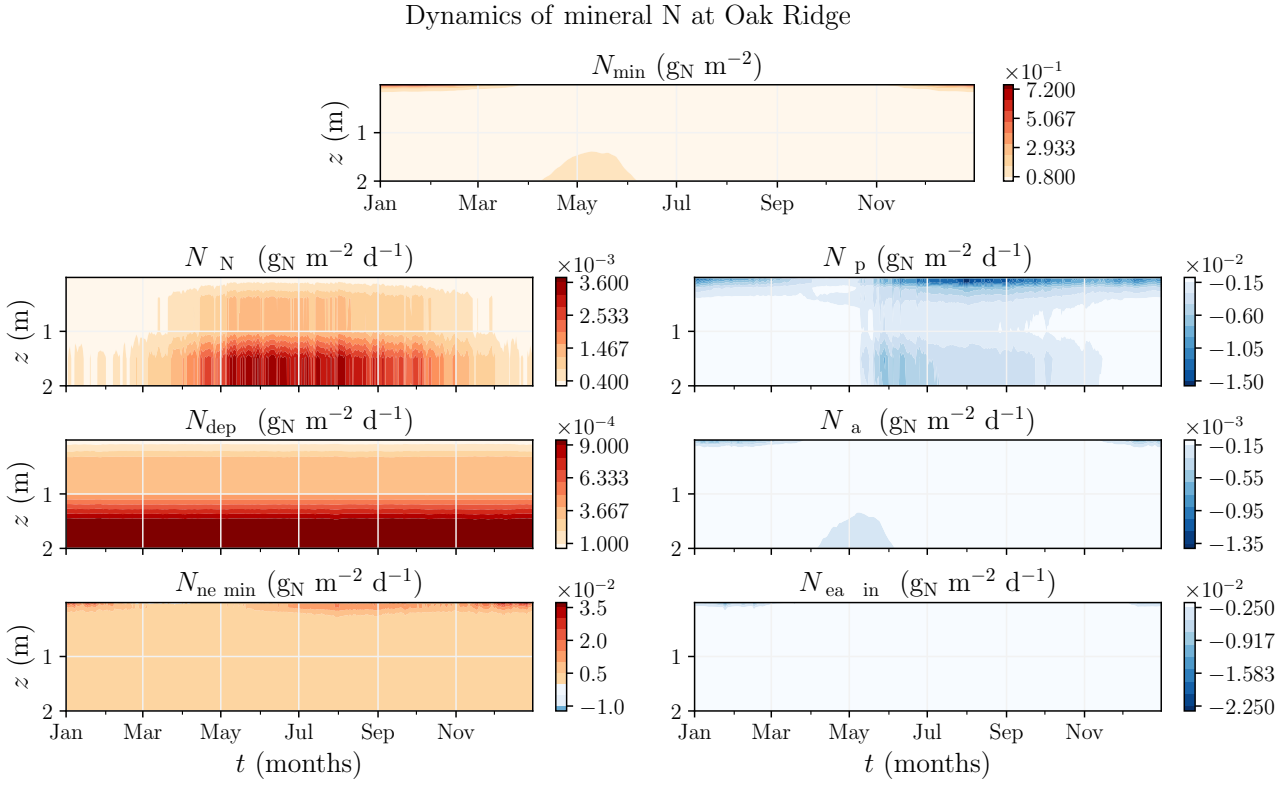

Figure A3. Seasonal cycle of soil profile of N fluxes and mineral pool at Oak Ridge for the reference plot exposed to ambient CO_2 concentration.

Author contributions. JD did the model development, modeling and wrote the paper. RD gave expertise on the N cycle and reviewed the paper. CD and BD supervised the project, gave their expertise on modeling and reviewed the paper.

Competing interests. The authors declare no conflict of interest.

Acknowledgements. This research was funded by the European Union's Horizon 2020 (H2020) research and innovation program under Grant Agreement No. 101003536 (ESM2025-Earth System Models for the Future). This study has also received funding from Agence Nationale de la Recherche - France 2030 as part of the PEPR TRACCS programme under grant number ANR-22-EXTR-0009. The authors are grateful for the forcing files provided by the H2020 project CRESCENDO Coordinated Research in Earth Systems and Climate: Experiments,

https://doi.org/10.5194/egusphere-2026-791
Preprint. Discussion started: 10 April 2026

580 Knowledge, Dissemination and Outreach, which received funding from the European Union Horizon 2020 research and innovation program under grant agreement no 641816. The authors thank Roland Séférian for his valuable feedback and constructive comments.

Financial support. This research was funded by the European Union's Horizon 2020 (H2020) research and innovation program under Grant Agreement No. 101003536 (ESM2025-Earth System Models for the Future). This study has also received funding from Agence Nationale de la Recherche - France 2030 as part of the PEPR TRACCS programme under grant number ANR-22-EXTR-0009.

https://doi.org/10.5194/egusphere-2026-791
Preprint. Discussion started: 10 April 2026

References

Ackermann, K., Zackrisson, O., Rousk, J., Jones, D. L., and DeLuca, T. H.: N2 Fixation in Feather Mosses Is a Sensitive Indicator of N Deposition in Boreal Forests, Ecosystems, 15, 986–998, https://doi.org/10.1007/s10021-012-9562-y, 2012.

Arora, V. K., Katavouta, A., Williams, R. G., Jones, C. D., Brovkin, V., Friedlingstein, P., Schwinger, J., Bopp, L., Boucher, O., Cadule, P., Chamberlain, M. A., Christian, J. R., Delire, C., Fisher, R. A., Hajima, T., Ilyina, T., Joetzjer, E., Kawamiya, M., Koven, C. D., Krasting, J. P., Law, R. M., Lawrence, D. M., Lenton, A., Lindsay, K., Pongratz, J., Raddatz, T., Séférian, R., Tachiiri, K., Tjiputra, J. F., Wiltshire, A., Wu, T., and Ziehn, T.: Carbon–Concentration and Carbon–Climate Feedbacks in CMIP6 Models and Their Comparison to CMIP5 Models, Biogeosciences, 17, 4173–4222, https://doi.org/10.5194/bg-17-4173-2020, 2020.

Bellenger, J. P., Darnajoux, R., Zhang, X., and Kraepiel, A. M. L.: Biological Nitrogen Fixation by Alternative Nitrogenases in Terrestrial Ecosystems: A Review, Biogeochemistry, 149, 53–73, https://doi.org/10.1007/s10533-020-00666-7, 2020.

Calvet, J.-C., Noilhan, J., Roujean, J.-L., Bessemoulin, P., Cabelguenne, M., Olioso, A., and Wigneron, J.-P.: An Interactive Vegetation SVAT Model Tested against Data from Six Contrasting Sites, Agricultural and Forest Meteorology, 92, 73–95, https://doi.org/10.1016/S0168-1923(98)00091-4, 1998.

Cleveland, C. C., Townsend, A. R., Schimel, D. S., Fisher, H., Howarth, R. W., Hedin, L. O., Perakis, S. S., Latty, E. F., Von Fischer, J. C., Elseroad, A., and Wasson, M. F.: Global Patterns of Terrestrial Biological Nitrogen (N_2) Fixation in Natural Ecosystems, Global Biogeochemical Cycles, 13, 623–645, https://doi.org/10.1029/1999GB900014, 1999.

Darnajoux, R., Reji, L., Zhang, X. R., Luxem, K. E., and Zhang, X.: Ammonium Sensitivity of Biological Nitrogen Fixation by Anaerobic Diazotrophs in Cultures and Benthic Marine Sediments, Journal of Geophysical Research: Biogeosciences, 127, e2021JG006 596, https://doi.org/10.1029/2021JG006596, 2022.

De Sisto, M. L., MacDougall, A. H., Mengis, N., and Antoniello, S.: Modelling the Terrestrial Nitrogen and Phosphorus Cycle in the UVic ESCM, Geoscientific Model Development, 16, 4113–4136, https://doi.org/10.5194/gmd-16-4113-2023, 2023.

Decayeux, J.: Representation of the Nitrogen Cycle and Its Coupling with the Carbon Cycle in ISBA (SURFEX v9) the Land Surface Model: Evaluation Using Two Free-Air CO_2 Enrichment Experiment Sites., 2026.

Decharme, B., Delire, C., Minvielle, M., Colin, J., Vergnes, J.-P., Alias, A., Saint-Martin, D., Séférian, R., Sénési, S., and Voldoire, A.: Recent Changes in the ISBA-CTRIP Land Surface System for Use in the CNRM-CM6 Climate Model and in Global Off-Line Hydrological Applications, Journal of Advances in Modeling Earth Systems, 11, 1207–1252, https://doi.org/10.1029/2018MS001545, 2019.

Delire, C., Séférian, R., Decharme, B., Alkama, R., Calvet, J.-C., Carrer, D., Gibelin, A.-L., Joetzjer, E., Morel, X., Rocher, M., and Tzanos, D.: The Global Land Carbon Cycle Simulated With ISBA-CTRIP: Improvements Over the Last Decade, Journal of Advances in Modeling Earth Systems, 12, e2019MS001 886, https://doi.org/10.1029/2019MS001886, 2020.

Dixon, R. and Kahn, D.: Genetic Regulation of Biological Nitrogen Fixation, Nature Reviews Microbiology, 2, 621–631, https://doi.org/10.1038/nrmicro954, 2004.

Drake, J. E., Gallet-Budynek, A., Hofmockel, K. S., Bernhardt, E. S., Billings, S. A., Jackson, R. B., Johnsen, K. S., Lichter, J., McCarthy, H. R., McCormack, M. L., Moore, D. J. P., Oren, R., Palmroth, S., Phillips, R. P., Pippen, J. S., Pritchard, S. G., Treseder, K. K., Schlesinger, W. H., DeLucia, E. H., and Finzi, A. C.: Increases in the Flux of Carbon Belowground Stimulate Nitrogen Uptake and Sustain the Long-Term Enhancement of Forest Productivity under Elevated CO2: C Fluxes Belowground and Long-Term FACE Productivity, Ecology Letters, 14, 349–357, https://doi.org/10.1111/j.1461-0248.2011.01593.x, 2011.

https://doi.org/10.5194/egusphere-2026-791
Preprint. Discussion started: 10 April 2026

Elser, J. J., Bracken, M. E., Cleland, E. E., Gruner, D. S., Harpole, W. S., Hillebrand, H., Ngai, J. T., Seabloom, E. W., Shurin, J. B., and Smith, J. E.: Global Analysis of Nitrogen and Phosphorus Limitation of Primary Producers in Freshwater, Marine and Terrestrial Ecosystems, Ecology Letters, 10, 1135–1142, https://doi.org/10.1111/j.1461-0248.2007.01113.x, 2007.

Finzi, A. C., DeLucia, E. H., Hamilton, J. G., Richter, D. D., and Schlesinger, W. H.: The Nitrogen Budget of a Pine Forest under Free Air CO2 Enrichment, Oecologia, 132, 567–578, https://doi.org/10.1007/s00442-002-0996-3, 2002.

Finzi, A. C., Moore, D. J. P., DeLucia, E. H., Lichter, J., Hofmockel, K. S., Jackson, R. B., Kim, H.-S., Matamala, R., McCarthy, H. R., Oren, R., Pippen, J. S., and Schlesinger, W. H.: PROGRESSIVE NITROGEN LIMITATION OF ECOSYSTEM PROCESSES UNDER ELEVATED CO_2 IN A WARM-TEMPERATE FOREST, Ecology, 87, 15–25, https://doi.org/10.1890/04-1748, 2006.

Finzi, A. C., Norby, R. J., Calfapietra, C., Gallet-Budynek, A., Gielen, B., Holmes, W. E., Hoosbeek, M. R., Iversen, C. M., Jackson, R. B., Kubiske, M. E., Ledford, J., Liberloo, M., Oren, R., Polle, A., Pritchard, S., Zak, D. R., Schlesinger, W. H., and Ceulemans, R.: Increases in Nitrogen Uptake Rather than Nitrogen-Use Efficiency Support Higher Rates of Temperate Forest Productivity under Elevated CO_2, Proceedings of the National Academy of Sciences, 104, 14 014–14 019, https://doi.org/10.1073/pnas.0706518104, 2007.

Fisher, J. B., Sitch, S., Malhi, Y., Fisher, R. A., Huntingford, C., and Tan, S.-Y.: Carbon Cost of Plant Nitrogen Acquisition: A Mechanistic, Globally Applicable Model of Plant Nitrogen Uptake, Retranslocation, and Fixation, Global Biogeochemical Cycles, 24, 2009GB003 621, https://doi.org/10.1029/2009GB003621, 2010.

Flechard, C. R., Ibrom, A., Skiba, U. M., de Vries, W., van Oijen, M., Cameron, D. R., Dise, N. B., Korhonen, J. F. J., Buchmann, N., Legout, A., Simpson, D., Sanz, M. J., Aubinet, M., Loustau, D., Montagnani, L., Neirynck, J., Janssens, I. A., Pihlatie, M., Kiese, R., Siemens, J., Francez, A.-J., Augustin, J., Varlagin, A., Olejnik, J., Juszczak, R., Aurela, M., Berveiller, D., Chojnicki, B. H., Dämmgen, U., Delpierre, N., Djuricic, V., Drewer, J., Dufrêne, E., Eugster, W., Fauvel, Y., Fowler, D., Frumau, A., Granier, A., Gross, P., Hamon, Y., Helfter, C., Hensen, A., Horváth, L., Kitzler, B., Kruijt, B., Kutsch, W. L., Lobo-do-Vale, R., Lohila, A., Longdoz, B., Marek, M. V., Matteucci, G., Mitosinkova, M., Moreaux, V., Neftel, A., Ourcival, J.-M., Pilegaard, K., Pita, G., Sanz, F., Schjoerring, J. K., Sebastià, M.-T., Tang, Y. S., Uggerud, H., Urbaniak, M., van Dijk, N., Vesala, T., Vidic, S., Vincke, C., Weidinger, T., Zechmeister-Boltenstern, S., Butterbach-Bahl, K., Nemitz, E., and Sutton, M. A.: Carbon–Nitrogen Interactions in European Forests and Semi-Natural Vegetation – Part 1: Fluxes and Budgets of Carbon, Nitrogen and Greenhouse Gases from Ecosystem Monitoring and Modelling, Biogeosciences, 17, 1583–1620, https://doi.org/10.5194/bg-17-1583-2020, 2020.

Fleischer, K. and Terrer, C.: Estimates of Soil Nutrient Limitation on the CO_2 Fertilization Effect for Tropical Vegetation, Global Change Biology, 28, 6366–6369, https://doi.org/10.1111/gcb.16377, 2022.

Friedlingstein, P., O'Sullivan, M., Jones, M. W., Andrew, R. M., Hauck, J., Landschützer, P., Le Quéré, C., Li, H., Luijkx, I. T., Olsen, A., Peters, G. P., Peters, W., Pongratz, J., Schwingshackl, C., Sitch, S., Canadell, J. G., Ciais, P., Jackson, R. B., Alin, S. R., Arneth, A., Arora, V., Bates, N. R., Becker, M., Bellouin, N., Berghoff, C. F., Bittig, H. C., Bopp, L., Cadule, P., Campbell, K., Chamberlain, M. A., Chandra, N., Chevallier, F., Chini, L. P., Colligan, T., Decayeux, J., Djeutchouang, L., Dou, X., Duran Rojas, C., Enyo, K., Evans, W., Fay, A., Feely, R. A., Ford, D. J., Foster, A., Gasser, T., Gehlen, M., Gkritzalis, T., Grassi, G., Gregor, L., Gruber, N., Gürses, Ö., Harris, I., Hefner, M., Heinke, J., Hurtt, G. C., Iida, Y., Ilyina, T., Jacobson, A. R., Jain, A., Jarníková, T., Jersild, A., Jiang, F., Jin, Z., Kato, E., Keeling, R. F., Klein Goldewijk, K., Knauer, J., Korsbakken, J. I., Lauvset, S. K., Lefèvre, N., Liu, Z., Liu, J., Ma, L., Maksyutov, S., Marland, G., Mayot, N., McGuire, P., Metzl, N., Monacci, N. M., Morgan, E. J., Nakaoka, S.-I., Neill, C., Niwa, Y., Nützel, T., Olivier, L., Ono, T., Palmer, P. I., Pierrot, D., Qin, Z., Resplandy, L., Roobaert, A., Rosan, T. M., Rödenbeck, C., Schwinger, J., Smallman, T. L., Smith, S., Sospedra-Alfonso, R., Steinhoff, T., Sun, Q., Sutton, A. J., Séférian, R., Takao, S., Tatebe, H., Tian, H., Tilbrook, B., Torres,

https://doi.org/10.5194/egusphere-2026-791
Preprint. Discussion started: 10 April 2026

O., Tourigny, E., Tsujino, H., Tubiello, F., Van Der Werf, G., Wanninkhof, R., Wang, X., Yang, D., Yang, X., Yu, Z., Yuan, W., Yue, X., Zaehle, S., Zeng, N., and Zeng, J.: Global Carbon Budget 2024, https://doi.org/10.5194/essd-2024-519, 2024.

Galloway, J. N., Dentener, F. J., Capone, D. G., Boyer, E. W., Howarth, R. W., Seitzinger, S. P., Asner, G. P., Cleveland, C. C., Green, P. A., Holland, E. A., Karl, D. M., Michaels, A. F., Porter, J. H., Townsend, A. R., and Vosmarty, C. J.: Nitrogen Cycles: Past, Present, and Future, Biogeochemistry, 70, 153–226, https://doi.org/10.1007/s10533-004-0370-0, 2004.

Gibelin, A.-L., Calvet, J.-C., and Viovy, N.: Modelling Energy and CO2 Fluxes with an Interactive Vegetation Land Surface Model-Evaluation at High and Middle Latitudes, Agricultural and Forest Meteorology, 148, 1611–1628, https://doi.org/10.1016/j.agrformet.2008.05.013, 2008.

Goll, D. S., Brovkin, V., Parida, B. R., Reick, C. H., Kattge, J., Reich, P. B., van Bodegom, P. M., and Niinemets, Ü.: Nutrient Limitation Reduces Land Carbon Uptake in Simulations with a Model of Combined Carbon, Nitrogen and Phosphorus Cycling, Biogeosciences, 9, 3547–3569, https://doi.org/10.5194/bg-9-3547-2012, 2012.

Hamiton, J. G., DeLucia, E. H., George, K., Naidu, S. L., Finzi, A. C., and Schlesinger, W. H.: Forest Carbon Balance under Elevated CO2, Ecosystems ecology, 2002.

Hendrey, G. R., Ellsworth, D. S., Lewin, K. F., and Nagy, JohN.: A Free-air Enrichment System for Exposing Tall Forest Vegetation to Elevated Atmospheric CO $_2$, Global Change Biology, 5, 293–309, https://doi.org/10.1046/j.1365-2486.1999.00228.x, 1999.

Ingwersen, J., Butterbach-Bahl, K., Gasche, R., Richter, O., and Papen, H.: Barometric Process Separation: New Method for Quantifying Nitrification, Denitrification, and Nitrous Oxide Sources in Soils, Soil Science Society of America Journal, 63, 117–128, https://doi.org/10.2136/sssaj1999.03615995006300010018x, 1999.

Iversen, C. M., Keller, J. K., Garten, C. T., and Norby, R. J.: Soil Carbon and Nitrogen Cycling and Storage throughout the Soil Profile in a Sweetgum Plantation after 11 Years of CO $_2$ -enrichment, Global Change Biology, 18, 1684–1697, https://doi.org/10.1111/j.1365-2486.2012.02643.x, 2012.

Jacobs, C. M. J.: Direct impact of atmospheric Co2 entrichment on regional transpiration, Ph.D. thesis, Agricultural University, Wageningen, 1994.

Jain, A., Yang, X., Kheshgi, H., McGuire, A. D., Post, W., and Kicklighter, D.: Nitrogen Attenuation of Terrestrial Carbon Cycle Response to Global Environmental Factors: NITROGEN ATTENUATION OF CARBON CYCLE, Global Biogeochemical Cycles, 23, n/a–n/a, https://doi.org/10.1029/2009GB003519, 2009.

Jastrow, J. D., Michael Miller, R., Matamala, R., Norby, R. J., Boutton, T. W., Rice, C. W., and Owensby, C. E.: Elevated Atmospheric Carbon Dioxide Increases Soil Carbon, Global Change Biology, 11, 2057–2064, https://doi.org/10.1111/j.1365-2486.2005.01077.x, 2005.

Joetzjer, E., Delire, C., Douville, H., Ciais, P., Decharme, B., Carrer, D., Verbeeck, H., De Weirdt, M., and Bonal, D.: Improving the ISBAcc Land Surface Model Simulation of Water and Carbon Fluxes and Stocks over the Amazon Forest, Geoscientific Model Development, 8, 1709–1727, https://doi.org/10.5194/gmd-8-1709-2015, 2015.

Johnson, D. W.: Progressive N Limitation in Forests: Review and Implications for Long-Term Responses to Elevated CO2, Ecology, pp. 64–75, 2006.

Johnson, D. W., Cheng, W., Joslin, J. D., Norby, R. J., Edwards, N. T., and Todd, D. E.: Effects of Elevated CO $_2$ on Nutrient Cycling in a Sweetgum Plantation, Biogeochemistry, 69, 379–403, https://doi.org/10.1023/B:BIOG.0000031054.19158.7c, 2004.

Khalil, K., Mary, B., and Renault, P.: Nitrous Oxide Production by Nitrification and Denitrification in Soil Aggregates as Affected by O2 Concentration, Soil Biology and Biochemistry, 36, 687–699, https://doi.org/10.1016/j.soilbio.2004.01.004, 2004.

https://doi.org/10.5194/egusphere-2026-791
Preprint. Discussion started: 10 April 2026

Kou-Giesbrecht, S. and Arora, V. K.: Representing the Dynamic Response of Vegetation to Nitrogen Limitation via Biological Nitrogen Fixation in the CLASSIC Land Model, Global Biogeochemical Cycles, 36, e2022GB007 341, https://doi.org/10.1029/2022GB007341, 2022.

Kou-Giesbrecht, S., Arora, V. K., Seiler, C., Arneth, A., Falk, S., Jain, A. K., Joos, F., Kennedy, D., Knauer, J., Sitch, S., O'Sullivan, M., Pan, N., Sun, Q., Tian, H., Vuichard, N., and Zaehle, S.: Evaluating Nitrogen Cycling in Terrestrial Biosphere Models: A Disconnect between the Carbon and Nitrogen Cycles, Earth System Dynamics, 14, 767–795, https://doi.org/10.5194/esd-14-767-2023, 2023.

Kronzucker, H. J., Siddiqi, M. Y., and Class, A. D. M.: Kinetics of NH,+ Lnflux in Spruce', Plant Physiology, 110, 773–779, 1996.

Lamarque, J.-F., Kyle, G. P., Meinshausen, M., Riahi, K., Smith, S. J., van Vuuren, D. P., Conley, A. J., and Vitt, F.: Global and Regional Evolution of Short-Lived Radiatively-Active Gases and Aerosols in the Representative Concentration Pathways, Climatic Change, 109, 191–212, https://doi.org/10.1007/s10584-011-0155-0, 2011.

Li, C., Frolking, S., and Frolking, T. A.: A Model of Nitrous Oxide Evolution from Soil Driven by Rainfall Events: 1. Model Structure and Sensitivity, Journal of Geophysical Research: Atmospheres, 97, 9759–9776, https://doi.org/10.1029/92JD00509, 1992.

Li, C., Aber, J., Stange, F., Butterbach-Bahl, K., and Papen, H.: A Process-Oriented Model of N $_2$ O and NO Emissions from Forest Soils: 1. Model Development, Journal of Geophysical Research: Atmospheres, 105, 4369–4384, https://doi.org/10.1029/1999JD900949, 2000.

Liang, J., Qi, X., Souza, L., and Luo, Y.: Processes Regulating Progressive Nitrogen Limitation under Elevated Carbon Dioxide: A Meta-Analysis, Biogeosciences, 13, 2689–2699, https://doi.org/10.5194/bg-13-2689-2016, 2016.

Lichter, J., Barron, S. H., Bevacqua, C. E., Finzi, A. C., Irving, K. E., Stemmler, E. A., and Schlesinger, W. H.: SOIL CARBON SEQUESTRATION AND TURNOVER IN A PINE FOREST AFTER SIX YEARS OF ATMOSPHERIC CO2 ENRICHMENT, Ecology, 86, 1835–1847, 2005.

Luo, Y., Su, B., Currie, W. S., Dukes, J. S., Finzi, A., Hartwig, U., Hungate, B., Mc Murtrie, R. E., Oren, R., Parton, W. J., Pataki, D. E., Shaw, M. R., Zak, D. R., and Field, C. B.: Progressive Nitrogen Limitation of Ecosystem Responses to Rising Atmospheric Carbon Dioxide, BioScience, 54, 731, https://doi.org/10.1641/0006-3568(2004)054[0731:PNLOER]2.0.CO;2, 2004.

McCarthy, H. R., Oren, R., Johnsen, K. H., Gallet-Budynek, A., Pritchard, S. G., Cook, C. W., LaDeau, S. L., Jackson, R. B., and Finzi, A. C.: Re-assessment of Plant Carbon Dynamics at the Duke Free-air CO $_2$ Enrichment Site: Interactions of Atmospheric [CO $_2$] with Nitrogen and Water Availability over Stand Development, New Phytologist, 185, 514–528, https://doi.org/10.1111/j.1469-8137.2009.03078.x, 2010.

Meyerholt, J., Sickel, K., and Zaehle, S.: Ensemble Projections Elucidate Effects of Uncertainty in Terrestrial Nitrogen Limitation on Future Carbon Uptake, Global Change Biology, 26, 3978–3996, https://doi.org/10.1111/gcb.15114, 2020.

Morel, X., Decharme, B., Delire, C., Krinner, G., Lund, M., Hansen, B. U., and Mastepanov, M.: A New Process-Based Soil Methane Scheme: Evaluation Over Arctic Field Sites With the ISBA Land Surface Model, Journal of Advances in Modeling Earth Systems, 11, 293–326, https://doi.org/10.1029/2018MS001329, 2019.

Norby, R. J. and Iversen, C. M.: NITROGEN UPTAKE, DISTRIBUTION, TURNOVER, AND EFFICIENCY OF USE IN A CO $_2$ -ENRICHED SWEETGUM FOREST, Ecology, 87, 5–14, https://doi.org/10.1890/04-1950, 2006.

Norby, R. J., Hanson, P. J., O'Neill, E. G., Tschaplinski, T. J., Weltzin, J. F., Hansen, R. A., Cheng, W., Wullschleger, S. D., Gunderson, C. A., Edwards, N. T., and Johnson, D. W.: NET PRIMARY PRODUCTIVITY OF A CO2-ENRICHED DECIDUOUS FOREST AND THE IMPLICATIONS FOR CARBON STORAGE, Ecological Applications, 12, 2002.

https://doi.org/10.5194/egusphere-2026-791
Preprint. Discussion started: 10 April 2026

Norby, R. J., Warren, J. M., Iversen, C. M., Medlyn, B. E., and McMurtrie, R. E.: CO $_2$ Enhancement of Forest Productivity Constrained by Limited Nitrogen Availability, Proceedings of the National Academy of Sciences, 107, 19 368–19 373, https://doi.org/10.1073/pnas.1006463107, 2010.

Pan, Y., Birdsey, R. A., Fang, J., Houghton, R., Kauppi, P. E., Kurz, W. A., Phillips, O. L., Shvidenko, A., Lewis, S. L., Canadell, J. G., Ciais, P., Jackson, R. B., Pacala, S. W., McGuire, A. D., Piao, S., Rautiainen, A., Sitch, S., and Hayes, D.: A Large and Persistent Carbon Sink in the World's Forests, Science, 333, 988–993, https://doi.org/10.1126/science.1201609, 2011.

Parton, W. J., Stewart, J. W. B., and Cole, C. V.: Dynamics of C, N, P and S in Grassland Soils: A Model, Biogeochemistry, 5, 109–131, https://doi.org/10.1007/BF02180320, 1988.

Parton, W. J., Mosier, A. R., Ojima, D. S., Valentine, D. W., Schimel, D. S., Weier, K., and Kulmala, A. E.: Generalized Model for N $_2$ and N $_2$ O Production from Nitrification and Denitrification, Global Biogeochemical Cycles, 10, 401–412, https://doi.org/10.1029/96GB01455, 1996.

Reick, C. H., Gayler, V., Goll, D., Hagemann, S., Heidkamp, M., Nabel, J. E. M. S., Raddatz, T., Roeckner, E., Schnur, R., and Wilkenskjeld, S.: JSBACH 3 - The Land Component of the MPI Earth System Model: Documentation of Version 3.2, Berichte zur Erdsystemforschung, https://doi.org/10.17617/2.3279802, 2021.

Reis Ely, C. R., Perakis, S. S., Cleveland, C. C., Menge, D. N. L., Reed, S. C., Taylor, B. N., Batterman, S. A., Clark, C. M., Crews, T. E., Dynarski, K. A., Gei, M., Gundale, M. J., Herridge, D. F., Jovan, S. E., Kou-Giesbrecht, S., Peoples, M. B., Piipponen, J., Rodríguez-Caballero, E., Salmon, V. G., Soper, F. M., Staccone, A. P., Weber, B., Williams, C. A., and Wurzburger, N.: Global Terrestrial Nitrogen Fixation and Its Modification by Agriculture, Nature, 643, 705–711, https://doi.org/10.1038/s41586-025-09201-w, 2025.

Schlesinger, W. H.: Biogeochemistry, an Analysis of Global Change, Academic Press, second edn., ISBN 0-12-625155-X, 1997.

Schlüter, S., Lucas, M., Grosz, B., Ippisch, O., Zawallich, J., He, H., Dechow, R., Kraus, D., Blagodatsky, S., Senbayram, M., Kravchenko, A., Vogel, H.-J., and Well, R.: The Anaerobic Soil Volume as a Controlling Factor of Denitrification: A Review, Biology and Fertility of Soils, 61, 343–365, https://doi.org/10.1007/s00374-024-01819-8, 2025.

Séférian, R., Nabat, P., Michou, M., Saint-Martin, D., Voldoire, A., Colin, J., Decharme, B., Delire, C., Berthet, S., Chevallier, M., Sénési, S., Franchisteguy, L., Vial, J., Mallet, M., Joetzjer, E., Geoffroy, O., Guérémy, J.-F., Moine, M.-P., Msadek, R., Ribes, A., Rocher, M., Roehrig, R., Salas-y Mélia, D., Sanchez, E., Terray, L., Valcke, S., Waldman, R., Aumont, O., Bopp, L., Deshayes, J., Éthé, C., and Madec, G.: Evaluation of CNRM Earth System Model, CNRM-ESM2-1: Role of Earth System Processes in Present-Day and Future Climate, Journal of Advances in Modeling Earth Systems, 11, 4182–4227, https://doi.org/10.1029/2019MS001791, 2019.

Sitch, S., O'Sullivan, M., Robertson, E., Friedlingstein, P., Albergel, C., Anthoni, P., Arneth, A., Arora, V. K., Bastos, A., Bastrikov, V., Bellouin, N., Canadell, J. G., Chini, L., Ciais, P., Falk, S., Harris, I., Hurtt, G., Ito, A., Jain, A. K., Jones, M. W., Joos, F., Kato, E., Kennedy, D., Klein Goldewijk, K., Kluzek, E., Knauer, J., Lawrence, P. J., Lombardozzi, D., Melton, J. R., Nabel, J. E. M. S., Pan, N., Peylin, P., Pongratz, J., Poulter, B., Rosan, T. M., Sun, Q., Tian, H., Walker, A. P., Weber, U., Yuan, W., Yue, X., and Zaehle, S.: Trends and Drivers of Terrestrial Sources and Sinks of Carbon Dioxide: An Overview of the TRENDY Project, Global Biogeochemical Cycles, 38, e2024GB008 102, https://doi.org/10.1029/2024GB008102, 2024.

Sparks, J. P., Walker, J., Turnipseed, A., and Guenther, A.: Dry Nitrogen Deposition Estimates over a Forest Experiencing Free Air CO $_2$ Enrichment, Global Change Biology, 14, 768–781, https://doi.org/10.1111/j.1365-2486.2007.01526.x, 2008.

Stocker, B. D., Dong, N., Perkowski, E. A., Schneider, P. D., Xu, H., De Boer, H. J., Rebel, K. T., Smith, N. G., Van Sundert, K., Wang, H., Jones, S. E., Prentice, I. C., and Harrison, S. P.: Empirical Evidence and Theoretical Understanding of Ecosystem Carbon and Nitrogen Cycle Interactions, New Phytologist, 245, 49–68, https://doi.org/10.1111/nph.20178, 2025.

https://doi.org/10.5194/egusphere-2026-791
Preprint. Discussion started: 10 April 2026

Sulman, B. N., Shevliakova, E., Brzostek, E. R., Kivlin, S. N., Malyshev, S., Menge, D. N., and Zhang, X.: Diverse Mycorrhizal Associations Enhance Terrestrial C Storage in a Global Model, Global Biogeochemical Cycles, 33, 501–523, https://doi.org/10.1029/2018GB005973, 2019.

Tagesson, T., Schurgers, G., Horion, S., Ciais, P., Tian, F., Brandt, M., Ahlström, A., Wigneron, J.-P., Ardö, J., Olin, S., Fan, L., Wu, Z., and Fensholt, R.: Recent Divergence in the Contributions of Tropical and Boreal Forests to the Terrestrial Carbon Sink, Nature Ecology & Evolution, 4, 202–209, https://doi.org/10.1038/s41559-019-1090-0, 2020.

Tegeder, M. and Masclaux-Daubresse, C.: Source and Sink Mechanisms of Nitrogen Transport and Use, New Phytologist, 217, 35–53, https://doi.org/10.1111/nph.14876, 2018.

Thomas, R. Q., Brookshire, E. N. J., and Gerber, S.: Nitrogen Limitation on Land: How Can It Occur in Earth System Models?, Global Change Biology, 21, 1777–1793, https://doi.org/10.1111/gcb.12813, 2015.

Thornton, P. E., Lamarque, J.-F., Rosenbloom, N. A., and Mahowald, N. M.: Influence of Carbon-Nitrogen Cycle Coupling on Land Model Response to CO_2 Fertilization and Climate Variability: INFLUENCE OF CARBON-NITROGEN COUPLING, Global Biogeochemical Cycles, 21, n/a–n/a, https://doi.org/10.1029/2006GB002868, 2007.

Thum, T., Caldararu, S., Engel, J., Kern, M., Pallandt, M., Schnur, R., Yu, L., and Zaehle, S.: A New Model of the Coupled Carbon, Nitrogen, and Phosphorus Cycles in the Terrestrial Biosphere (QUINCY v1.0; Revision 1996), Geoscientific Model Development, 12, 4781–4802, https://doi.org/10.5194/gmd-12-4781-2019, 2019.

Vitousek, P. M., Fahey, T., Johnson, D. W., and Swift, M. J.: Element Interactions in Forest Ecosystems: Succession, Allometry and Input-Output Budgets, Biogeochemistry, 5, 7–34, https://doi.org/10.1007/BF02180316, 1988.

Vitousek, PeterM. and Howarth, RobertW.: Nitrogen Limitation on Land and in the Sea: How Can It Occur?, Biogeochemistry, 13, https://doi.org/10.1007/BF00002772, 1991.

Voldoire, A., Saint-Martin, D., Sénési, S., Decharme, B., Alias, A., Chevallier, M., Colin, J., Guérémy, J.-F., Michou, M., Moine, M.-P., Nabat, P., Roehrig, R., Salas Y Mélia, D., Séférian, R., Valcke, S., Beau, I., Belamari, S., Berthet, S., Cassou, C., Cattiaux, J., Deshayes, J., Douville, H., Ethé, C., Franchistéguy, L., Geoffroy, O., Lévy, C., Madec, G., Meurdesoif, Y., Msadek, R., Ribes, A., Sanchez-Gomez, E., Terray, L., and Waldman, R.: Evaluation of CMIP6 DECK Experiments With CNRM-CM6-1, Journal of Advances in Modeling Earth Systems, 11, 2177–2213, https://doi.org/10.1029/2019MS001683, 2019.

Vuichard, N., Messina, P., Luyssaert, S., Guenet, B., Zaehle, S., Ghattas, J., Bastrikov, V., and Peylin, P.: Accounting for Carbon and Nitrogen Interactions in the Global Terrestrial Ecosystem Model ORCHIDEE (Trunk Version, Rev 4999): Multi-Scale Evaluation of Gross Primary Production, Geoscientific Model Development, 12, 4751–4779, https://doi.org/10.5194/gmd-12-4751-2019, 2019.

White, M. A., Thornton, P. E., Running, S. W., and Nemani, R. R.: Parameterization and Sensitivity Analysis of the BIOME–BGC Terrestrial Ecosystem Model: Net Primary Production Controls, Earth Interactions, 4, 1–85, https://doi.org/10.1175/1087-3562(2000)004<0003:PASAOT>2.0.CO;2, 2000.

Wieder, W. R., Cleveland, C. C., Lawrence, D. M., and Bonan, G. B.: Effects of Model Structural Uncertainty on Carbon Cycle Projections: Biological Nitrogen Fixation as a Case Study, Environmental Research Letters, 10, 044 016, https://doi.org/10.1088/1748-9326/10/4/044016, 2015a.

Wieder, W. R., Cleveland, C. C., Smith, W. K., and Todd-Brown, K.: Future Productivity and Carbon Storage Limited by Terrestrial Nutrient Availability, Nature Geoscience, 8, 441–444, https://doi.org/10.1038/ngeo2413, 2015b.

https://doi.org/10.5194/egusphere-2026-791
Preprint. Discussion started: 10 April 2026

Wiltshire, A. J., Burke, E. J., Chadburn, S. E., Jones, C. D., Cox, P. M., Davies-Barnard, T., Friedlingstein, P., Harper, A. B., Liddicoat, S., Sitch, S., and Zaehle, S.: JULES-CN: A Coupled Terrestrial Carbon–Nitrogen Scheme (JULES Vn5.1), Geoscientific Model Development, 14, 2161–2186, https://doi.org/10.5194/gmd-14-2161-2021, 2021.

Xu-Ri and Prentice, I. C.: Terrestrial Nitrogen Cycle Simulation with a Dynamic Global Vegetation Model, Global Change Biology, 14, 1745–1764, https://doi.org/10.1111/j.1365-2486.2008.01625.x, 2008.

Yang, X., Wittig, V., Jain, A. K., and Post, W.: Integration of Nitrogen Cycle Dynamics into the Integrated Science Assessment Model for the Study of Terrestrial Ecosystem Responses to Global Change: INTEGRATION OF NITROGEN DYNAMICS, Global Biogeochemical Cycles, 23, n/a–n/a, https://doi.org/10.1029/2009GB003474, 2009.

Yin, X.: Responses of Leaf Nitrogen Concentration and Specific Leaf Area to Atmospheric CO2 Enrichment: A Retrospective Synthesis across 62 Species, Global Change Biology, 8, 631–642, https://doi.org/10.1046/j.1365-2486.2002.00497.x, 2002.

Zaehle, S. and Friend, A. D.: Carbon and Nitrogen Cycle Dynamics in the O-CN Land Surface Model: 1. Model Description, Site-Scale Evaluation, and Sensitivity to Parameter Estimates, Global Biogeochemical Cycles, 24, n/a–n/a, https://doi.org/10.1029/2009GB003521, 2010.

Zaehle, S., Medlyn, B. E., De Kauwe, M. G., Walker, A. P., Dietze, M. C., Hickler, T., Luo, Y., Wang, Y.-P., El-Masri, B., Thornton, P., Jain, A., Wang, S., Warlind, D., Weng, E., Parton, W., Iversen, C. M., Gallet-Budynek, A., McCarthy, H., Finzi, A., Hanson, P. J., Prentice, I. C., Oren, R., and Norby, R. J.: Evaluation of 11 Terrestrial Carbon–Nitrogen Cycle Models against Observations from Two Temperate F Ree- A Ir CO $_2$ E Nrichment Studies, New Phytologist, 202, 803–822, https://doi.org/10.1111/nph.12697, 2014.